PLOS | ONE

RESEARCH ARTICLE

Mixed Convective Peristaltic Flow of Water Based Nanofluids with Joule Heating and Convective Boundary Conditions

Tasawar Hayat[1,2], Sadaf Nawaz[1]*, Ahmed Alsaedi[2], Maimona Rafiq[1]

1 Department of Mathematics, Quaid-I-Azam University 45320, Islamabad 44000, Pakistan, **2** Nonlinear Analysis and Applied Mathematics (NAAM) Research Group, Department of Mathematics, Faculty of Sciences, King Abdulaziz University, Jeddah 21589, Saudi Arabia

* sadafnawaz26@gmail.com

Abstract

Main objective of present study is to analyze the mixed convective peristaltic transport of water based nanofluids using five different nanoparticles i.e. (Al_2O_3, CuO, Cu, Ag and TiO_2). Two thermal conductivity models namely the Maxwell's and Hamilton-Crosser's are used in this study. Hall and Joule heating effects are also given consideration. Convection boundary conditions are employed. Furthermore, viscous dissipation and heat generation/absorption are used to model the energy equation. Problem is simplified by employing lubrication approach. System of equations are solved numerically. Influence of pertinent parameters on the velocity and temperature are discussed. Also the heat transfer rate at the wall is observed for considered five nanofluids using the two phase models via graphs.

CrossMark
click for updates

OPEN ACCESS

Citation: Hayat T, Nawaz S, Alsaedi A, Rafiq M (2016) Mixed Convective Peristaltic Flow of Water Based Nanofluids with Joule Heating and Convective Boundary Conditions. PLoS ONE 11(4): e0153537. doi:10.1371/journal.pone.0153537

Editor: Bing-Yang Cao, Tsinghua University, CHINA

Received: January 8, 2016

Accepted: March 17, 2016

Published: April 22, 2016

Copyright: © 2016 Hayat et al. This is an open access article distributed under the terms of the Creative Commons Attribution License, which permits unrestricted use, distribution, and reproduction in any medium, provided the original author and source are credited.

Data Availability Statement: All relevant data are within the paper.

Funding: The authors received no specific funding for this work.

Competing Interests: The authors have declared that no competing interests exist.

Introduction

Nanofluid is a type of fluid engineered by dispersing nanometer size materials e.g. nanoparticles, nanorods, nanotubes and so on in conventional fluids like water, ethylene-glycol and oil etc. Up to now, much more attention has been given to the potentials of nanofluids in practical applications among these heat transfer enhancement is the most significant issue. The term nanofluids was initially used by Choi [1]. The commonly used nanoparticles are metals (Cu, Ag, Fe, Au), metallic oxides (CuO, Al_2O_3, TiO_2, ZnO), nitride/carbide ceramics (AlN, SiN, SiC, TiC), and carbon nanotubes etc. The most commonly used base fluids are water, ethylene-glycol and oil etc. Because of the property of enhancing the heat transfer rate the nanofluids are extensively used in automobiles as coolant. In welding equipments, nanofluids are used to cool high heat-flux devices such as high power microwave tubes and high power laser diode arrays. The measurement of nanofluids critical heat flux (CHF) in a forced convection loop is very useful for nuclear applications. Wide variety of industrial applications ranging from transportation to energy production, electronic systems like microprocessors, Micro-Electro-Mechanical Systems (MEMS) and biotechnology involves the use of nanofluids. Some of the investigations on the nanofluids are given through the references [2–10]. Several models are used to estimate

the thermal conductivity of nanofluids. However, Maxwell's [11] and Hamilton Crosser's [12] models are extensively used.

Peristaltic mechanism is important in physiology for the transport of fluids. This mechanism is induced due to the sinusoidal wave along the walls which propel the fluid. It is extensively found in the human body for the transport of food through esophagus, transport of urine from kidneys to bladder, fluid mechanics in the perivascular space of the brain etc. Besides these it is used in industry for sanitary fluid transport. Many devices for example heart lung machine, hose pump, peristalsis pump etc, are operated under this principle. Transport of water to all branches of tree are due to the same principle. Due to these developments the peristalsis has become an important topic for research and some literature in this regard can be seen through the references [13–26].

Due to the advancement in medical science many diseases are cured by the use of colloidal drug delivery. In the drug delivery system with the help of magnetic fluxes the magnetic nanoparticles with the drug are sent to the tumor side. With the help of applied magnetic field it is possible to control the magnetic-nanoparticles in the human body towards the tumor site. Now a days in the modern drug delivery system the peristaltic transport of nanofluid has gained the attention. Some studies dealing with the peristaltic flows of nanofluids can be consulted through the studies [27–35].

In this study mixed convective peristaltic transport of water based nanofluids is considered. Influence of constant applied magnetic field in an asymmetric channel is taken into account. Moreover Joule heating is accounted. Study is done for the spherical and cylindrical nanoparticles. Viscous dissipation and heat generation/absorption are also considered. Convective boundary conditions are utilized. System of equations are solved numerically. The results are analyzed for the various parameters of interest.

Modeling

An incompressible water-based nanofluid filling an asymmetric channel of width d_1+d_2 (see Fig 1) is considered. Nanofluids are the suspension of Titanium oxide or titania (TiO_2), Aluminum oxide or Alumina (Al_2O_3), Copper oxide (CuO), Copper (Cu) and Silver (Ag) and water. Moreover base fluid and nanoparticles are considered thermally consistent with respect to each other. Magnetic field of strength B_0 is applied in a direction normal to flow. Induced magnetic field for small magnetic Reynolds number is ignored.

The Lorentz force is given by

$$\boldsymbol{F} = \boldsymbol{J} \times \boldsymbol{B},$$

where $\mathbf{B} = [0,0,B_0]$ and $\boldsymbol{J}$ denotes the applied magnetic field and current density respectively. By considering the Hall effects the current density can be represented as follows:

$$\boldsymbol{J} = \sigma_{eff}[\boldsymbol{E} + \boldsymbol{V} \times \boldsymbol{B} - \frac{1}{en_e}[\boldsymbol{J} \times \boldsymbol{B}]].$$

Here σ_{eff} denotes the effective electric conductivity of nanofluid, **E** is the electric field, the velocity field $\boldsymbol{V} = [\bar{U}(\bar{X},\bar{Y},\bar{t}),\ \bar{V}(\bar{X},\bar{Y},\bar{t}),0]$, e represents the electron charge and n_e the number density of free electrons. Here applied and the induced electric fields are taken zero and thus

$$\boldsymbol{J} = \sigma_{eff}[\boldsymbol{V} \times \boldsymbol{B} - \frac{1}{en_e}[\boldsymbol{J} \times \boldsymbol{B}]].$$

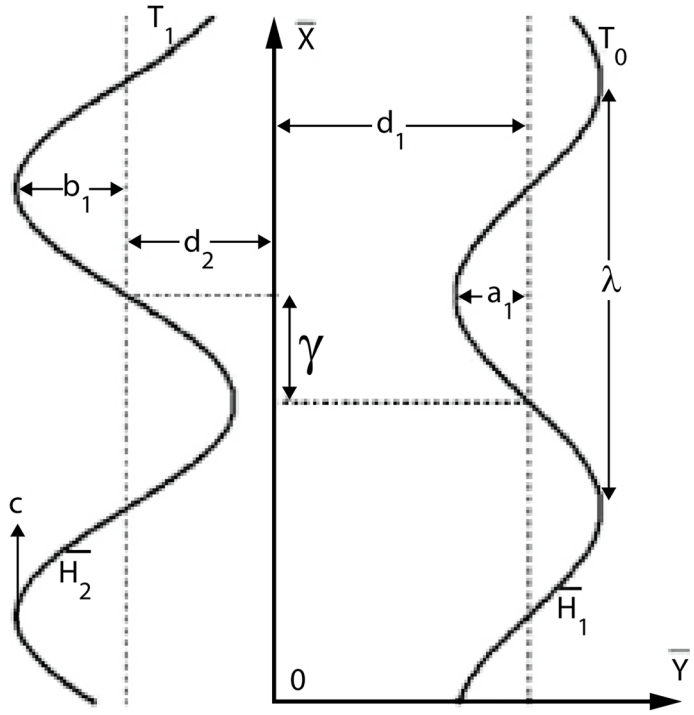

Fig 1. Problem sketch.

doi:10.1371/journal.pone.0153537.g001

The Lorentz force is given by

$$\boldsymbol{F} = \left[\frac{\sigma_{eff}{B_0}^2}{1+\left(\frac{\sigma_{eff}B_0}{en_e}\right)^2}\left(-\bar{U}+\left(\frac{\sigma_{eff}B_0}{en_e}\right)\bar{V}\right),\ \frac{-\sigma_{eff}{B_0}^2}{1+\left(\frac{\sigma_{eff}B_0}{en_e}\right)^2}\left(\bar{V}+\left(\frac{\sigma_{eff}B_0}{en_e}\right)\bar{U}\right),0\right].$$

The effective electric conductivity of nanofluid for two-phase flow model is defined below [32]:

$$\frac{\sigma_{eff}}{\sigma_f} = 1+\frac{3\left(\frac{\sigma_p}{\sigma_f}-1\right)\phi}{\left(\frac{\sigma_p}{\sigma_f}+2\right)-\left(\frac{\sigma_p}{\sigma_f}-1\right)\phi}.$$

Here σ_p and σ_f are the electric conductivity of nanoparticles and water respectively and ϕ denote the nanoparticle volume fraction. Now we have

$$\boldsymbol{F} = \left[\frac{A_1\sigma_f{B_0}^2}{1+(A_1m)^2}(-\bar{U}+A_1m\bar{V}),\ \frac{-A_1\sigma_f{B_0}^2}{1+(A_1m)^2}(\bar{V}+A_1m\bar{U}),0\right],$$

where A_1 and the Hall parameter m is defined by:

$$m = \frac{\sigma_f B_0}{en_e}, A_1 = 1+\frac{3\left(\frac{\sigma_p}{\sigma_f}-1\right)\phi}{\left(\frac{\sigma_p}{\sigma_f}+2\right)-\left(\frac{\sigma_p}{\sigma_f}-1\right)\phi}.$$

The Joule heating is

$$\frac{1}{\sigma_{eff}}\boldsymbol{J}.\boldsymbol{J} = \frac{A_1\sigma_f {B_0}^2}{1+(A_1 m)^2}(\bar{U}^2+\bar{V}^2).$$

Now we select the Cartesian coordinate system such that $\bar{X}$ axis is along the length of channel and $\bar{Y}$ axis is perpendicular to it. Sinusoidal wave with constant speed c and wavelength λ propagate along the channel walls and hence generates the peristaltic flow. The shapes of travelling waves are represented by following relations:

$$\begin{aligned}\bar{H}_1(\bar{X},\bar{t}) &= d_1 + a_1\cos\frac{2\pi}{\lambda}(\bar{X}-c\bar{t}),\\ \bar{H}_2(\bar{X},\bar{t}) &= -d_2 - b_1\cos\left(\frac{2\pi}{\lambda}(\bar{X}-c\bar{t})+\gamma\right),\end{aligned} \tag{1}$$

where a_1 and b_1 are the wave amplitudes, γ the phase difference in the range $0 \le \gamma \le \pi$.

For the considered flow analysis the continuity equation is

$$\frac{\partial\bar{U}}{\partial\bar{X}} + \frac{\partial\bar{V}}{\partial\bar{Y}} = 0. \tag{2}$$

Velocity components in $\bar{X}$ and $\bar{Y}$ directions are

$$\begin{aligned}&\rho_{eff}\left(\frac{\partial}{\partial\bar{t}} + \bar{U}\frac{\partial}{\partial\bar{X}} + \bar{V}\frac{\partial}{\partial\bar{Y}}\right)\bar{U}\\ &\quad = -\frac{\partial\bar{P}}{\partial\bar{X}} + \mu_{eff}\left[\frac{\partial^2\bar{U}}{\partial\bar{X}^2} + \frac{\partial^2\bar{U}}{\partial\bar{Y}^2}\right] - \frac{A_1\sigma_f {B_0}^2}{1+(A_1 m)^2}(\bar{U}-A_1 m\bar{V}) + g(\rho\beta)_{eff}(T-T_m),\end{aligned} \tag{3}$$

$$\rho_{eff}\left(\frac{\partial}{\partial\bar{t}} + \bar{U}\frac{\partial}{\partial\bar{X}} + \bar{V}\frac{\partial}{\partial\bar{Y}}\right)\bar{V} = -\frac{\partial\bar{P}}{\partial\bar{Y}} + \mu_{eff}\left[\frac{\partial^2\bar{V}}{\partial\bar{X}^2} + \frac{\partial^2\bar{V}}{\partial\bar{Y}^2}\right] - \frac{A_1\sigma_f {B_0}^2}{1+(A_1 m)^2}(\bar{V}+A_1 m\bar{U}). \tag{4}$$

The energy equation with viscous dissipation and Joule heating effects is

$$\begin{aligned}&(\rho C)_{eff}\left(\frac{\partial}{\partial\bar{t}} + \bar{U}\frac{\partial}{\partial\bar{X}} + \bar{V}\frac{\partial}{\partial\bar{Y}}\right)T\\ &\quad = K_{eff}\left[\frac{\partial^2 T}{\partial\bar{X}^2} + \frac{\partial^2 T}{\partial\bar{Y}^2}\right] + \Phi + \mu_{eff}\left[2\left(\left(\frac{\partial\bar{U}}{\partial\bar{X}}\right)^2 + \left(\frac{\partial\bar{V}}{\partial\bar{Y}}\right)^2\right) + \left(\frac{\partial\bar{U}}{\partial\bar{Y}} + \frac{\partial\bar{V}}{\partial\bar{X}}\right)^2\right]\\ &\qquad + \frac{A_1\sigma_f {B_0}^2}{1+(A_1 m)^2}(\bar{U}^2+\bar{V}^2).\end{aligned} \tag{5}$$

Here $\bar{P}(\bar{X},\bar{Y},\bar{t})$ denotes the pressure, g denotes the acceleration due to gravity, $T_m = \frac{T_0+T_1}{2}$ the mean temperature and Φ is the dimensional heat generation/absorption parameter. The effective density ρ_{eff}, specific heat C_{eff}, effective viscosity and thermal expansion coefficient for

Table 1. Thermophysical parameters of water and nanoparticles [34].

	ρ (kg m^{-3})	C_p (j kg^{-1} K^{-1})	K (Wm^{-1}K^{-1})	β (l/k) × 10^{-6}	σ (Ω.*m*)$^{-1}$
H_2O	997.1	4179	0.613	210	0.05
TiO_2	4250	686.2	8.9538	9.0	1 × 10^{-12}
Al_2O_3	3970	765	40	8.5	1 × 10^{-10}
CuO	6320	531.8	76.5	18.0	2.7 × 10^{-8}
Cu	8933	385	401	16.7	5.96 × 10^{7}
Ag	10500	235	429	18.9	6.3 × 10^{7}

doi:10.1371/journal.pone.0153537.t001

the two-phase flow model are [33]:

$$\rho_{eff} = (1-\phi)\rho_f + \phi\rho_p, \quad (\rho C)_{eff} = (1-\phi)(\rho C)_f + \phi(\rho C)_p,$$

$$(\rho\beta)_{eff} = (1-\phi)\rho_f\beta_f + \phi\rho_p\beta_p, \quad \mu_{eff} = \frac{\mu_f}{(1-\phi)^{2.5}}.$$

The effective thermal conductivity for Maxwell's and Hamilton-Crosser's model is defined as follows:

$$\frac{K_{eff}}{K_f} = \frac{K_p + 2K_f - 2\phi(K_f - K_p)}{K_p + 2K_f + \phi(K_f - K_p)}, \tag{6}$$

[11] for Maxwell's model and

$$\frac{K_{eff}}{K_f} = \frac{K_p + (n-1)K_f - (n-1)\phi(K_f - K_p)}{K_p + (n-1)K_f + \phi(K_f - K_p)}, \tag{7}$$

[12] for Hamilton-Crosser's model

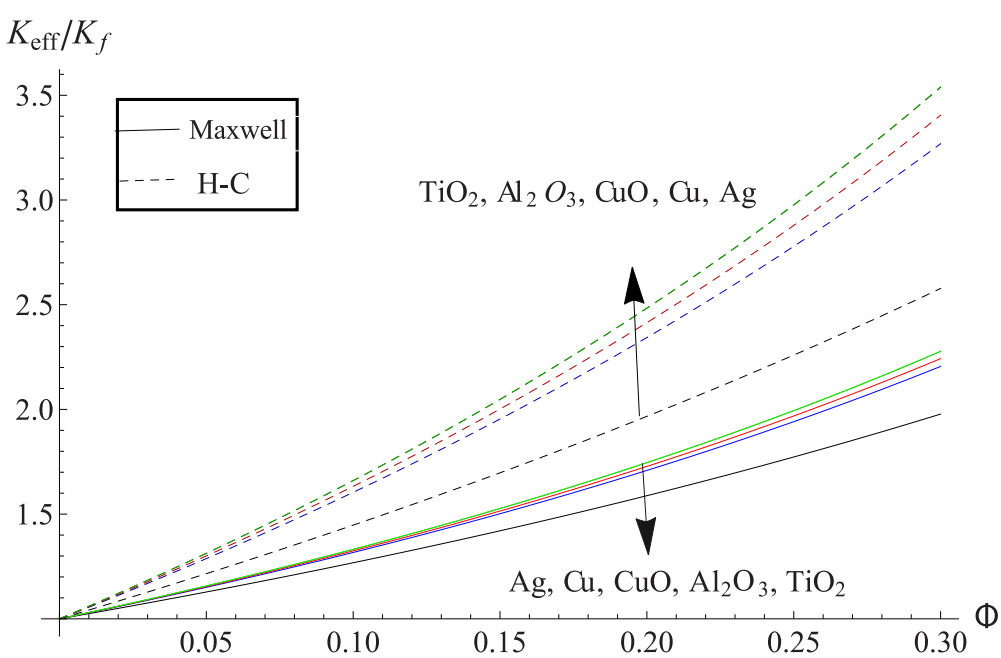

Fig 2. The effective thermal conductivity for Maxwell's and H-C's models.

doi:10.1371/journal.pone.0153537.g002

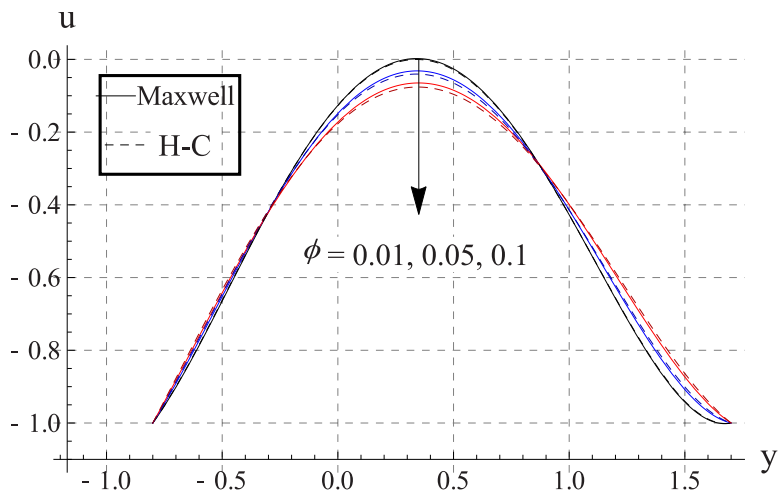

Fig 3. Effect of ϕ on axial velocity for TiO_2 when a = 0.7, b = 0.6, γ = π/2, d = 0.8, x = 0, η = 0.7, Br = 0.3, m = 2.0, M = 1.0, Bi_1 = 8, Bi_2 = 10, Gr = 3.0, ε = 2.5.

doi:10.1371/journal.pone.0153537.g003

where the subscripts *p* and *f* indicate the nanoparticle and fluid phases respectively.

Here *n* in Hamilton Crosser's represents the shape factor and its value is n = 3/ψ where ψ represents the sphericity of the nanoparticles. Here ψ = 0.5 and 1 correspond to the cylindrical and spherical nanoparticles. For *n* = 3 the Hamilton-Crosser's model reduces to the Maxwell's model.

The transformation between fixed and wave frames are given as follows:

$$\begin{aligned} &\bar{x} = \bar{X} - c\bar{t}, \quad \bar{y} = \bar{Y}, \quad \bar{u}(\bar{x},\bar{y}) = \bar{U}(\bar{X},\bar{Y},\bar{t}) - c, \\ &\bar{v}(\bar{x},\bar{y}) = \bar{V}(\bar{X},\bar{Y},\bar{t}), \quad \bar{p}(\bar{x},\bar{y}) = \bar{P}(\bar{X},\bar{Y},\bar{t}), \end{aligned} \tag{8}$$

After using the above transformations, the Eqs 2–5 become:

$$\frac{\partial \bar{u}}{\partial \bar{x}} + \frac{\partial \bar{v}}{\partial \bar{y}} = 0, \tag{9}$$

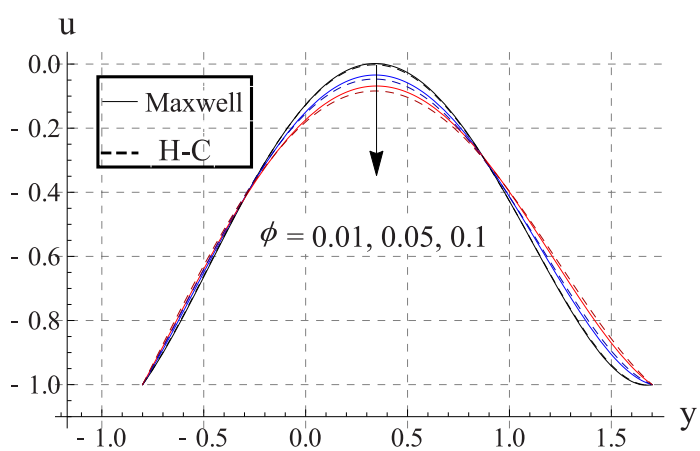

Fig 4. Effect of ϕ on axial velocity for Al_2O_3 when a = 0.7, b = 0.6, γ = π/2, d = 0.8, x = 0, η = 0.7, Br = 0.3, m = 2.0, M = 1.0, Bi_1 = 8, Bi_2 = 10, Gr = 3.0, ε = 2.5.

doi:10.1371/journal.pone.0153537.g004

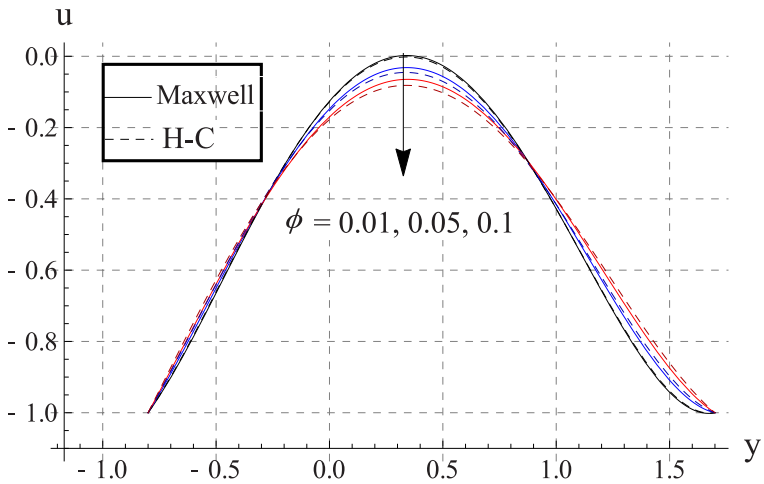

Fig 5. Effect of ϕ on axial velocity for CuO when a = 0.7, b = 0.6, γ = π/2, d = 0.8, x = 0, η = 0.7, Br = 0.3, m = 2.0, M = 1.0, Bi_1 = 8, Bi_2 = 10, Gr = 3.0, ε = 2.5.

doi:10.1371/journal.pone.0153537.g005

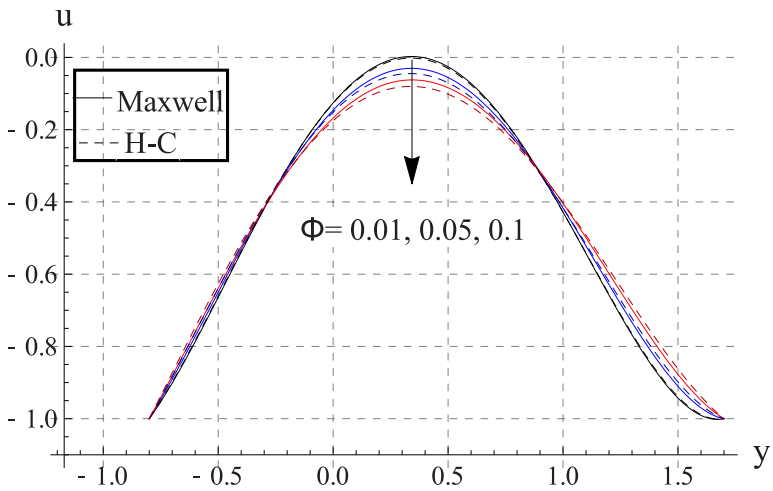

Fig 6. Effect of ϕ on axial velocity for Cu when a = 0.7, b = 0.6, γ = π/2, d = 0.8, x = 0, η = 0.7, Br = 0.3, m = 2.0, M = 1.0, Bi_1 = 8, Bi_2 = 10, Gr = 3.0, ε = 2.5.

doi:10.1371/journal.pone.0153537.g006

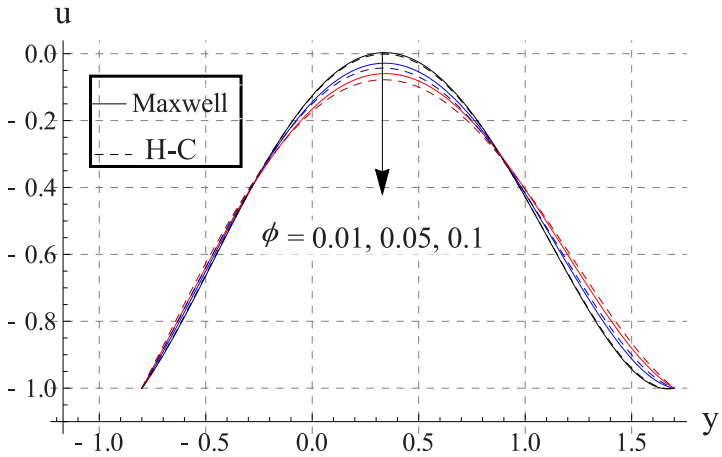

Fig 7. Effect of ϕ on axial velocity for Ag when a = 0.7, b = 0.6, γ = π/2, d = 0.8, x = 0, η = 0.7, Br = 0.3, m = 2.0, M = 1.0, Bi_1 = 8, Bi_2 = 10, Gr = 3.0, ε = 2.5.

doi:10.1371/journal.pone.0153537.g007

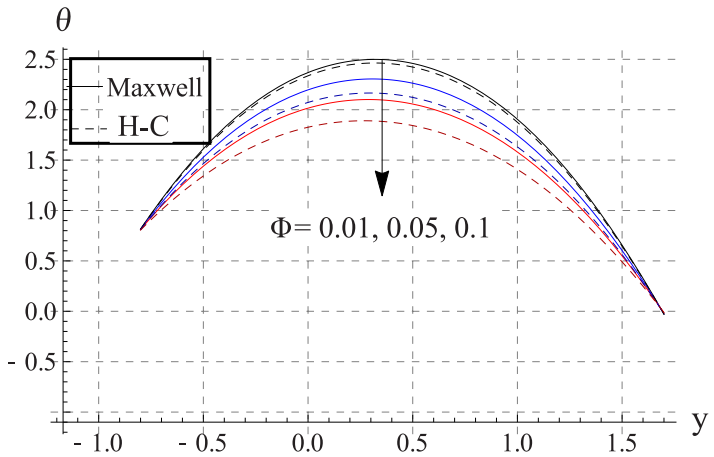

Fig 8. Effect of ϕ on temperature for TiO_2 when a = 0.7, b = 0.6, γ = π/2, d = 0.8, x = 0, η = 0.7, Br = 0.3, m = 2.0, M = 1.0, Bi_1 = 8, Bi_2 = 10, Gr = 3.0, ε = 2.5.

doi:10.1371/journal.pone.0153537.g008

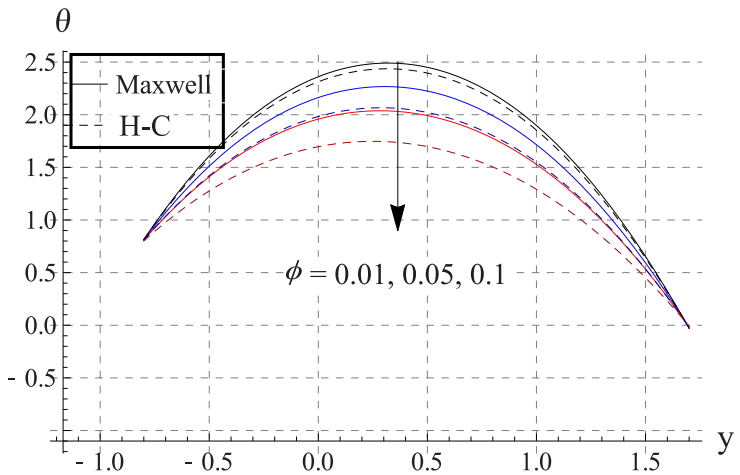

Fig 9. Effect of ϕ on temperature for Al_2O_3 when a = 0.7, b = 0.6, γ = π/2, d = 0.8, x = 0, η = 0.7, Br = 0.3, m = 2.0, M = 1.0, Bi_1 = 8, Bi_2 = 10, Gr = 3.0, ε = 2.5.

doi:10.1371/journal.pone.0153537.g009

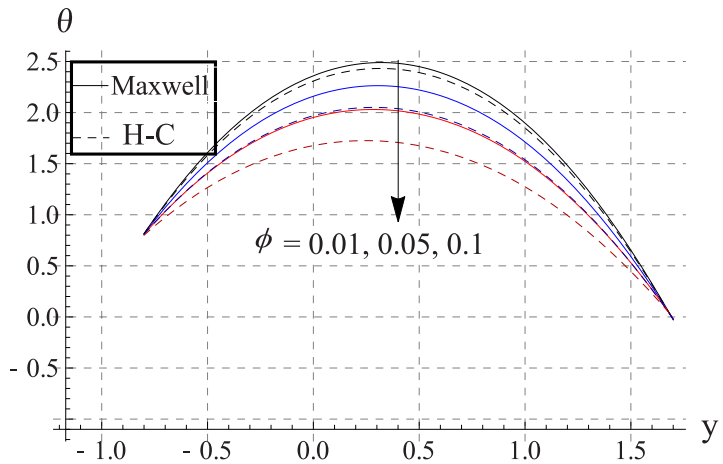

Fig 10. Effect of ϕ on temperature for CuO when a = 0.7, b = 0.6, γ = π/2, d = 0.8, x = 0, η = 0.7, Br = 0.3, m = 2.0, M = 1.0, Bi_1 = 8, Bi_2 = 10, Gr = 3.0, ε = 2.5.

doi:10.1371/journal.pone.0153537.g010

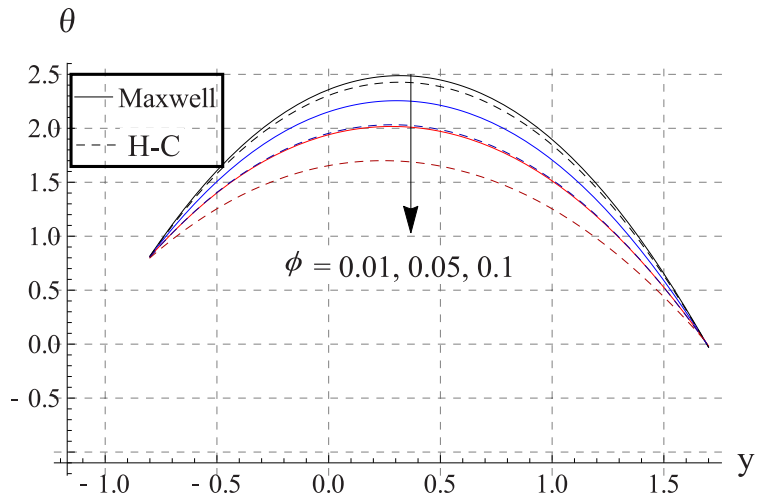

Fig 11. Effect of ϕ on temperature for Cu when a = 0.7, b = 0.6, γ = π/2, d = 0.8, x = 0, η = 0.7, Br = 0.3, m = 2.0, M = 1.0, Bi_1 = 8, Bi_2 = 10, Gr = 3.0, ε = 2.5.

doi:10.1371/journal.pone.0153537.g011

$$\begin{aligned}&\Big((1-\phi)\rho_f+\phi\rho_p\Big)\left((\bar{u}+c)\frac{\partial}{\partial\bar{x}}+\bar{v}\frac{\partial}{\partial\bar{y}}\right)(\bar{u}+c)\\&=-\frac{\partial\bar{p}}{\partial\bar{x}}+\frac{\mu_f}{(1-\phi)^{2.5}}\left[\frac{\partial^2\bar{u}}{\partial\bar{x}^2}+\frac{\partial^2\bar{u}}{\partial\bar{y}^2}\right]-\frac{A_1\sigma_f{B_0}^2}{1+(A_1m)^2}((\bar{u}+c)-A_1m\bar{v})\\&\quad+g\Big((1-\phi)\rho_f\beta_f+\phi\rho_p\beta_p\Big)(T-T_m),\end{aligned}\tag{10}$$

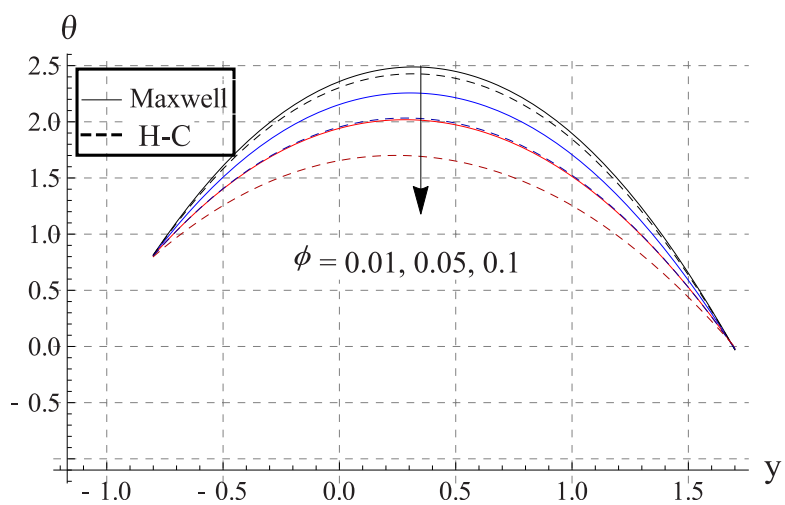

Fig 12. Effect of ϕ on temperature for Ag when a = 0.7, b = 0.6, γ = π/2, d = 0.8, x = 0, η = 0.7, Br = 0.3, m = 2.0, M = 1.0, Bi_1 = 8, Bi_2 = 10, Gr = 3.0, ε = 2.5.

doi:10.1371/journal.pone.0153537.g012

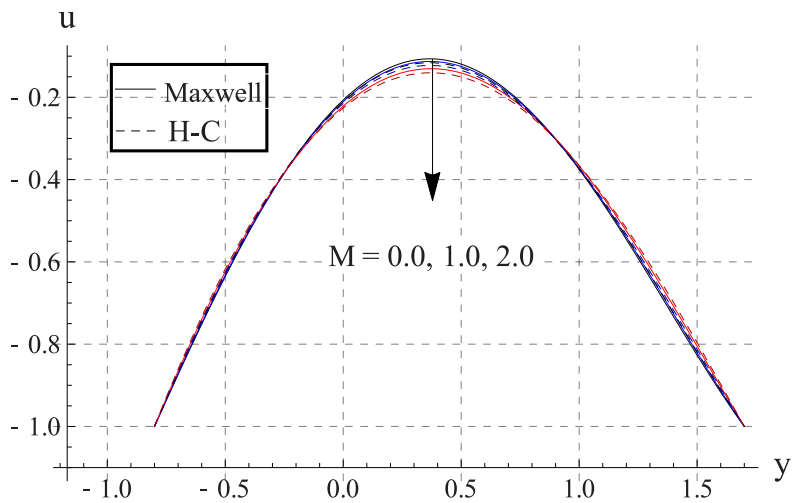

Fig 13. Effect of M on axial velocity for TiO_2 when a = 0.7, b = 0.6, γ = π/2, d = 0.8, x = 0, η = 0.7, Br = 0.3, m = 0.8, ϕ = 0.2, Bi_1 = 8, Bi_2 = 10, Gr = 3.0, ε = 2.5.

doi:10.1371/journal.pone.0153537.g013

$$\left((1-\phi)\rho_f+\phi\rho_p\right)\left((\bar{u}+c)\frac{\partial}{\partial\bar{x}}+\bar{v}\frac{\partial}{\partial\bar{y}}\right)(\bar{v})$$
$$=-\frac{\partial\bar{p}}{\partial\bar{y}}+\frac{\mu_f}{(1-\phi)^{2.5}}\left[\frac{\partial^2\bar{v}}{\partial\bar{x}^2}+\frac{\partial^2\bar{v}}{\partial\bar{y}^2}\right]-\frac{A_1\sigma_f B_0{}^2}{1+(A_1m)^2}(\bar{v}+A_1m(\bar{u}+c)), \tag{11}$$

$$\left((1-\phi)(\rho C)_f+\phi(\rho C)_p\right)\left((\bar{u}+c)\frac{\partial}{\partial\bar{x}}+\bar{v}\frac{\partial}{\partial\bar{y}}\right)T$$
$$=K_{eff}\left[\frac{\partial^2T}{\partial\bar{x}^2}+\frac{\partial^2T}{\partial\bar{y}^2}\right]+\Phi+\frac{\mu_f}{(1-\phi)^{2.5}}\left[2\left(\left(\frac{\partial\bar{u}}{\partial\bar{x}}\right)^2+\left(\frac{\partial\bar{v}}{\partial\bar{y}}\right)^2\right)+\left(\frac{\partial\bar{u}}{\partial\bar{y}}+\frac{\partial\bar{v}}{\partial\bar{x}}\right)^2\right]$$
$$+\frac{A_1\sigma_f B_0{}^2}{1+(A_1m)^2}((\bar{u}+c)^2+\bar{v}^2). \tag{12}$$

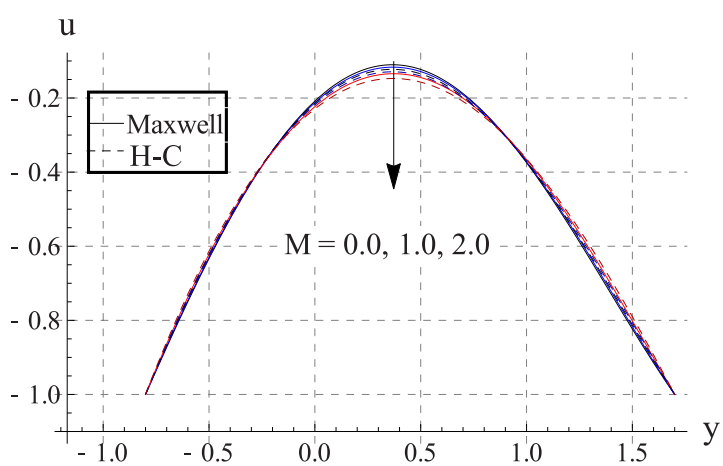

Fig 14. Effect of M on axial velocity for Al_2O_3 when a = 0.7, b = 0.6, γ = π/2, d = 0.8, x = 0, η = 0.7, Br = 0.3, m = 0.8, ϕ = 0.2, Bi_1 = 8, Bi_2 = 10, Gr = 3.0, ε = 2.5.

doi:10.1371/journal.pone.0153537.g014

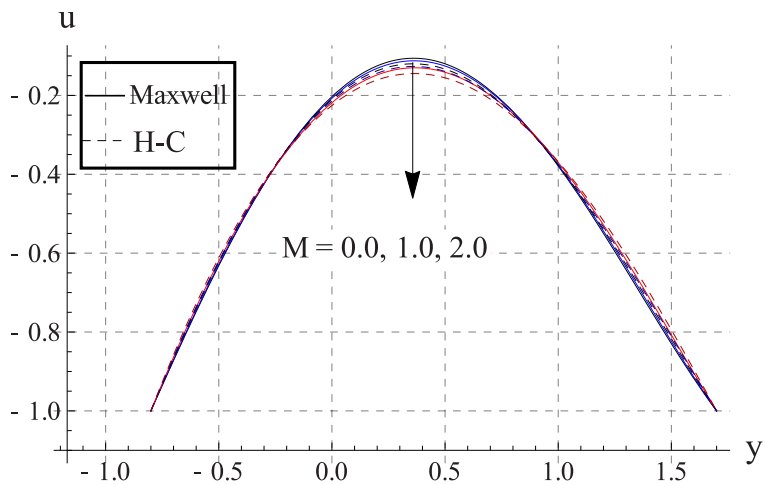

Fig 15. Effect of M on axial velocity for CuO when a = 0.7, b = 0.6, γ = π/2, d = 0.8, x = 0, η = 0.7, Br = 0.3, m = 0.8, ϕ = 0.2, Bi_1 = 8, Bi_2 = 10, Gr = 3.0, ε = 2.5.

doi:10.1371/journal.pone.0153537.g015

Numerical values of the thermophysical parameters of water and nanoparticles are mentioned in Table 1.

Non-dimensional quantities used in the above Eqs are

$$\begin{aligned} &x=\frac{\bar{x}}{\lambda},\ y=\frac{\bar{y}}{d_1},\ u=\frac{\bar{u}}{c},\ v=\frac{\bar{v}}{c\delta},\ \delta=\frac{d_1}{\lambda},\ h_1=\frac{\overline{H_1}}{d_1},\ h_2=\frac{\overline{H_2}}{d_1},\\ &d=\frac{d_2}{d_1},\ a=\frac{a_1}{d_1},\ b=\frac{b_1}{d_1},\ p=\frac{{d_1}^2\bar{p}}{c\lambda\mu_f},\ \theta=\frac{T-T_m}{T_{1-}T_0},\ Re=\frac{\rho_f c d_1}{\mu_f},\\ &Pr=\frac{\mu_f C_f}{K_f},\ Ec=\frac{c^2}{C_f(T_{1-}T_0)},\ Br=PrEc,\ Gr=\frac{g\rho_f\beta_f(T_{1-}T_0){d_1}^2}{c\mu_f},\\ &M=\sqrt{\frac{\sigma_f}{\mu_f}}B_0 d_1,\ \varepsilon=\frac{{d_1}^2\Phi}{(T_{1-}T_0)K_f},\ u=\frac{\partial\psi}{\partial y},\ v=-\frac{\partial\psi}{\partial x}, \end{aligned} \tag{13}$$

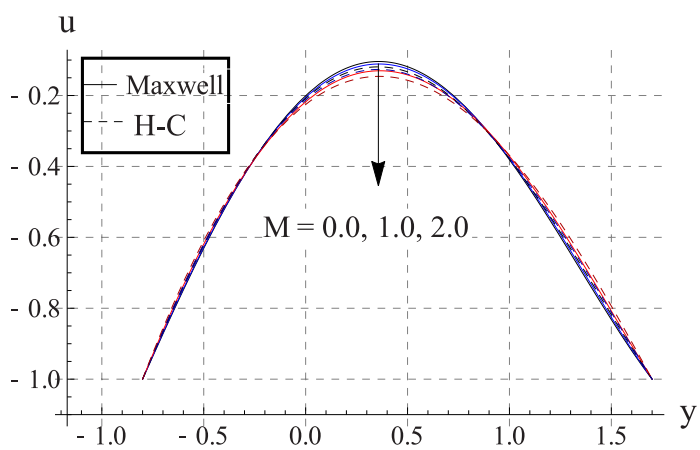

Fig 16. Effect of M on axial velocity for Cu when a = 0.7, b = 0.6, γ = π/2, d = 0.8, x = 0, η = 0.7, Br = 0.3, m = 0.8, ϕ = 0.2, Bi_1 = 8, Bi_2 = 10, Gr = 3.0, ε = 2.5.

doi:10.1371/journal.pone.0153537.g016

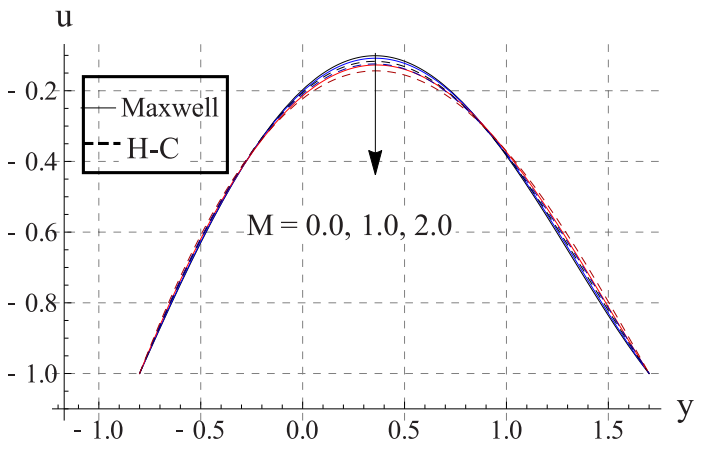

Fig 17. Effect of M on axial velocity for Ag when a = 0.7, b = 0.6, γ = π/2, d = 0.8, x = 0, η = 0.7, Br = 0.3, m = 0.8, ϕ = 0.2, Bi_1 = 8, Bi_2 = 10, Gr = 3.0, ε = 2.5.

doi:10.1371/journal.pone.0153537.g017

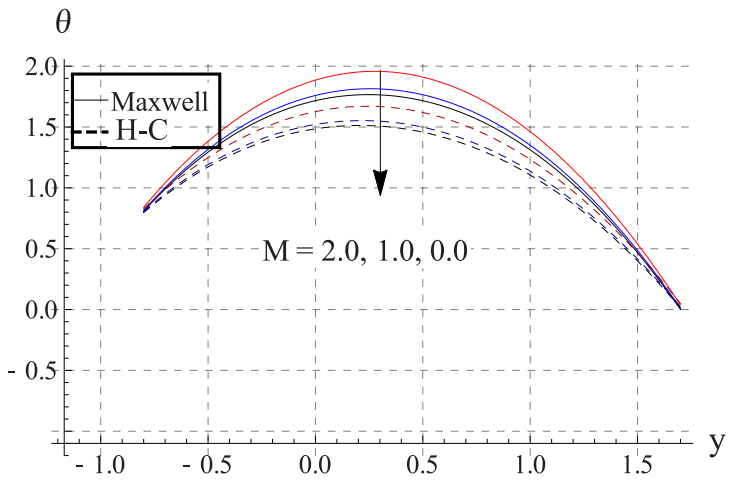

Fig 18. Effect of M on temperature for TiO_2 when a = 0.7, b = 0.6, γ = π/2, d = 0.8, x = 0, η = 0.7, Br = 0.3, m = 0.8, ϕ = 0.2, Bi_1 = 8, Bi_2 = 10, Gr = 3.0, ε = 2.5.

doi:10.1371/journal.pone.0153537.g018

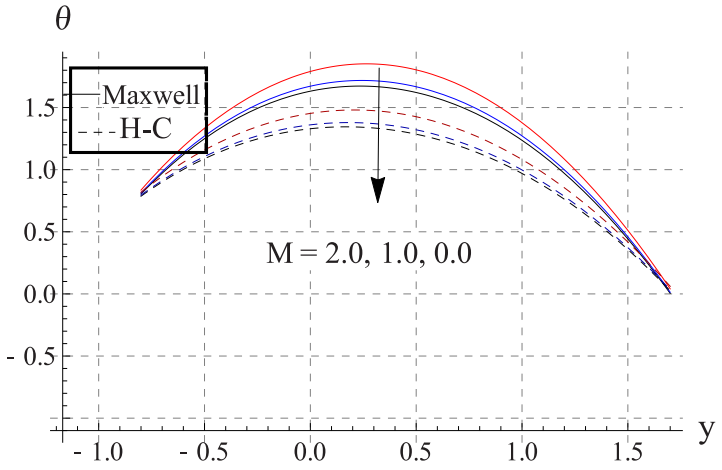

Fig 19. Effect of M on temperature for Al_2O_3 when a = 0.7, b = 0.6, γ = π/2, d = 0.8, x = 0, η = 0.7, Br = 0.3, m = 0.8, ϕ = 0.2, Bi_1 = 8, Bi_2 = 10, Gr = 3.0, ε = 2.5.

doi:10.1371/journal.pone.0153537.g019

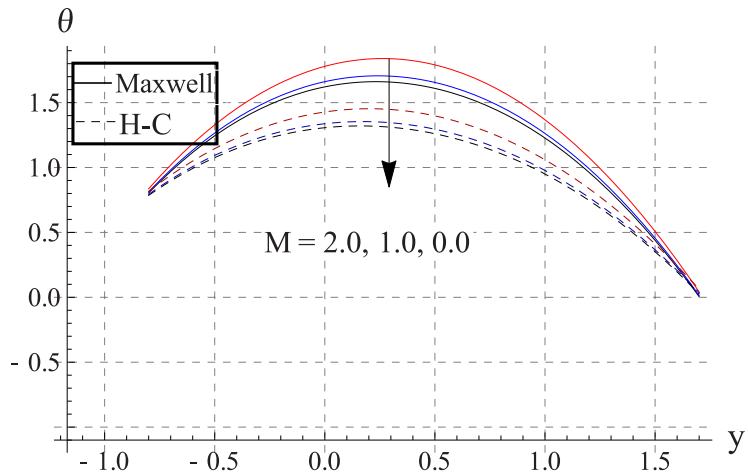

Fig 20. Effect of M on temperature for CuO when a = 0.7, b = 0.6, γ = π/2, d = 0.8, x = 0, η = 0.7, Br = 0.3, m = 0.8, ϕ = 0.2, Bi_1 = 8, Bi_2 = 10, Gr = 3.0, ε = 2.5.

doi:10.1371/journal.pone.0153537.g020

in which Re, Pr, Ec, Br, Gr, M represent the Reynolds, Prandtl, Eckert, Brinkman, Grashoff and Hartman numbers respectively whereas ε denotes the dimensionless heat generation/absorption.

After utilizing the lubrication approach, Eqs 10–12 take the form

$$\frac{\partial p}{\partial x} = \frac{1}{(1-\phi)^{2.5}}\frac{\partial^3 \psi}{\partial y^3} + A_2 Gr\theta - \frac{A_1 M^2}{1+(A_1 m)^2}\left(\frac{\partial \psi}{\partial y}+1\right), \tag{14}$$

$$\frac{\partial p}{\partial y} = 0, \tag{15}$$

$$A_3\frac{\partial^2 \theta}{\partial y^2} + \frac{Br}{(1-\phi)^{2.5}}\left(\frac{\partial^2 \psi}{\partial y^2}\right)^2 + \frac{BrA_1M^2}{1+(A_1 m)^2}\left(\frac{\partial \psi}{\partial y}+1\right)^2 + \varepsilon = 0, \tag{16}$$

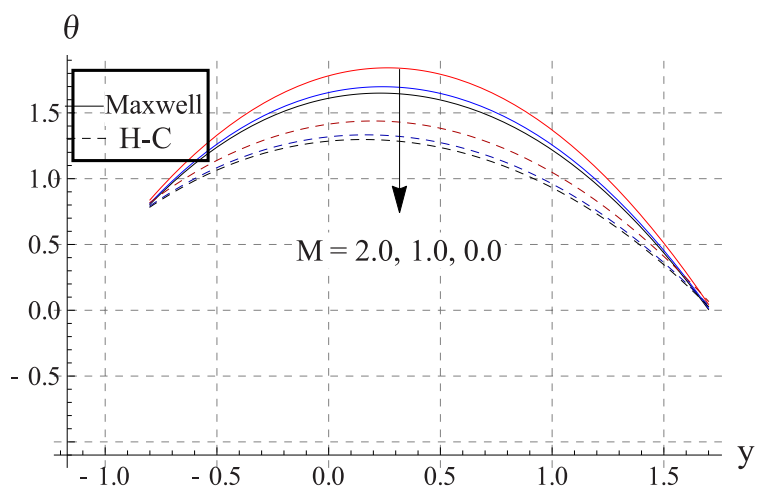

Fig 21. Effect of M on temperature for Cu when a = 0.7, b = 0.6, γ = π/2, d = 0.8, x = 0, η = 0.7, Br = 0.3, m = 0.8, ϕ = 0.2, Bi_1 = 8, Bi_2 = 10, Gr = 3.0, ε = 2.5.

doi:10.1371/journal.pone.0153537.g021

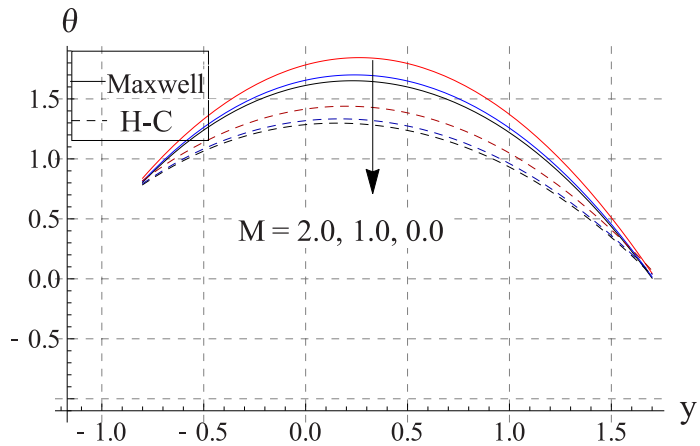

Fig 22. Effect of M on temperature for Ag when a = 0.7, b = 0.6, γ = π/2, d = 0.8, x = 0, η = 0.7, Br = 0.3, m = 0.8, ϕ = 0.2, Bi_1 = 8, Bi_2 = 10, Gr = 3.0, ε = 2.5.

doi:10.1371/journal.pone.0153537.g022

in which

$$A_1 = 1 + \frac{3\left(\frac{\sigma_p}{\sigma_f} - 1\right)\phi}{\left(\frac{\sigma_p}{\sigma_f} + 2\right) - \left(\frac{\sigma_p}{\sigma_f} - 1\right)\phi}, \; A_2 = 1 - \phi + \phi\left(\frac{(\rho\beta)_p}{(\rho\beta)_f}\right),$$

$$A_3 = \frac{K_p + 2K_f - 2\phi(K_f - K_p)}{K_p + 2K_f + \phi(K_f - K_p)},$$

[11] for Maxwell's model and

$$A_3 = \frac{K_p + (n-1)K_f - (n-1)\phi(K_f - K_p)}{K_p + (n-1)K_f + \phi(K_f - K_p)} \tag{17}$$

[12] for Hamilton-Crosser's model.

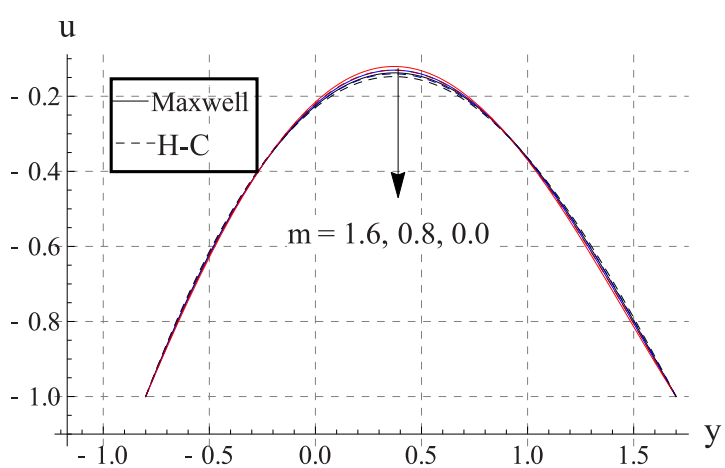

Fig 23. Effect of m on axial velocity for TiO_2 when a = 0.7, b = 0.6, γ = π/2, d = 0.8, x = 0, η = 0.7, Br = 0.3, ϕ = 0.2, M = 2.0, Bi_1 = 8, Bi_2 = 10, Gr = 3.0, ε = 2.5.

doi:10.1371/journal.pone.0153537.g023

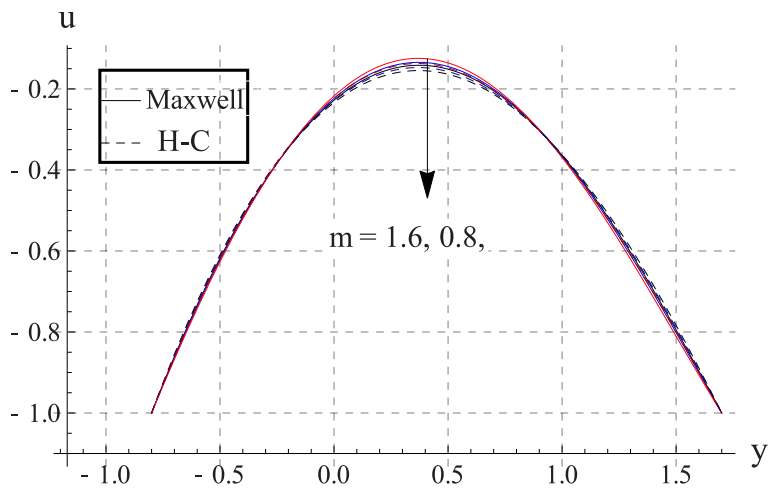

Fig 24. Effect of m on axial velocity for Al_2O_3 when a = 0.7, b = 0.6, γ = π/2, d = 0.8, x = 0, η = 0.7, Br = 0.3, ϕ = 0.2, M = 2.0, Bi_1 = 8, Bi_2 = 10, Gr = 3.0, ε = 2.5.

doi:10.1371/journal.pone.0153537.g024

Dimensionless flow rates in the laboratory η $(= \frac{\bar{Q}}{cd_1})$ and wave frames F $(= \frac{\bar{q}}{cd_1})$ are related by

$$\eta = F + 1 + d, \tag{18}$$

in which $\bar{Q}$ and $\bar{q}$ denote the dimensional flow rates in the laboratory and wave frames respectively and

$$F = \int_{h2}^{h1} \frac{\partial \psi}{\partial y}\, dy. \tag{19}$$

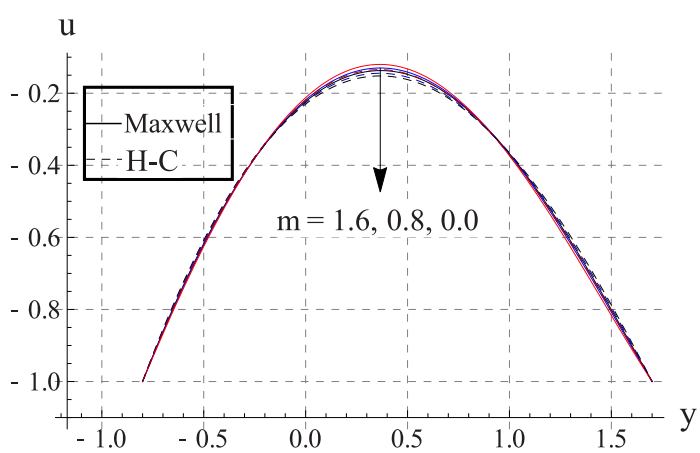

Fig 25. Effect of m on axial velocity for CuO when a = 0.7, b = 0.6, γ = π/2, d = 0.8, x = 0, η = 0.7, Br = 0.3, ϕ = 0.2, M = 2.0, Bi_1 = 8, Bi_2 = 10, Gr = 3.0, ε = 2.5.

doi:10.1371/journal.pone.0153537.g025

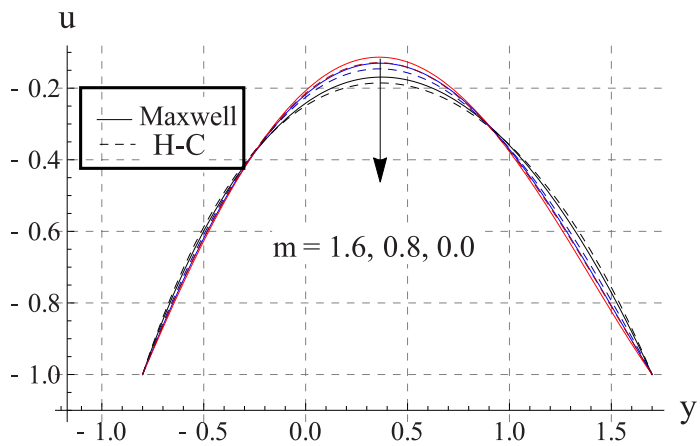

Fig 26. Effect of m on axial velocity for Cu when a = 0.7, b = 0.6, γ = π/2, d = 0.8, x = 0, η = 0.7, Br = 0.3, ϕ = 0.2, M = 2.0, Bi_1 = 8, Bi_2 = 10, Gr = 3.0, ε = 2.5.

doi:10.1371/journal.pone.0153537.g026

The no slip and convective conditions on the boundary are represented in the forms

$$\begin{aligned} &\bar{U} = 0, \quad K_{eff}\frac{\partial T}{\partial y} = -B_1(T - T_0) \;\; at\; \bar{Y} = \bar{H}_1(\bar{X}, \bar{t}), \\ &\bar{U} = 0, \;\; K_{eff}\frac{\partial T}{\partial y} = -B_2(T_1 - T) \;\; at\; \bar{Y} = \bar{H}_2(\bar{X}, \bar{t}), \end{aligned} \tag{20}$$

where, B_1 and B_2 are heat transfer coefficients at the walls respectively.

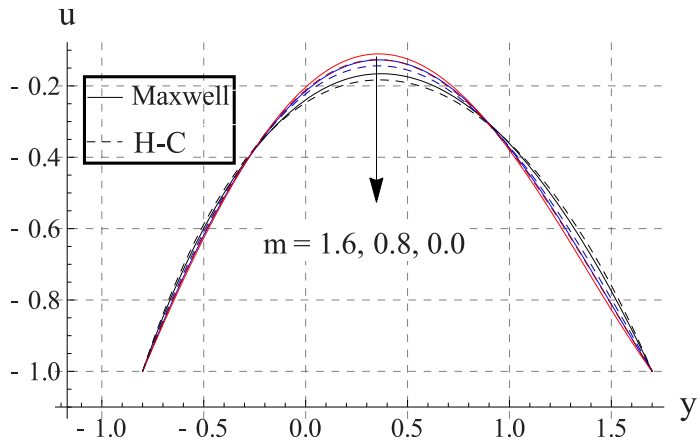

Fig 27. Effect of m on axial velocity for Ag when a = 0.7, b = 0.6, γ = π/2, d = 0.8, x = 0, η = 0.7, Br = 0.3, ϕ = 0.2, M = 2.0, Bi_1 = 8, Bi_2 = 10, Gr = 3.0, ε = 2.5.

doi:10.1371/journal.pone.0153537.g027

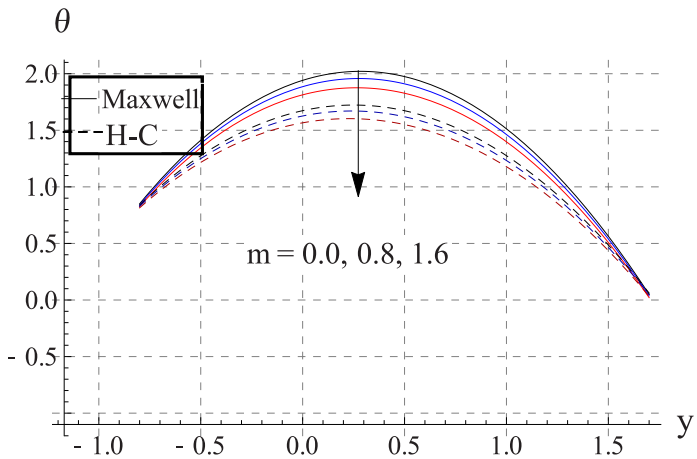

Fig 28. Effect of m on temperature for TiO_2 when a = 0.7, b = 0.6, γ = π/2, d = 0.8, x = 0, η = 0.7, Br = 0.3, ϕ = 0.2, M = 2.0, Bi_1 = 8, Bi_2 = 10, Gr = 3.0, ε = 2.5.

doi:10.1371/journal.pone.0153537.g028

The boundary conditions in dimensionless form are defined by:

$$\begin{aligned} &\psi = \frac{F}{2}, \quad \frac{\partial \psi}{\partial y} = -1, \quad \frac{\partial \theta}{\partial y} + \frac{Bi_1}{\left(\frac{K_{eff}}{K_f}\right)}\left(\theta + \frac{1}{2}\right) = 0 \ \ at\ y = h_1, \\ &\psi = -\frac{F}{2}, \quad \frac{\partial \psi}{\partial y} = -1, \quad \frac{\partial \theta}{\partial y} - \frac{Bi_2}{\left(\frac{K_{eff}}{K_f}\right)}\left(\theta - \frac{1}{2}\right) = 0 \ \ at\ y = h_2. \end{aligned} \tag{21}$$

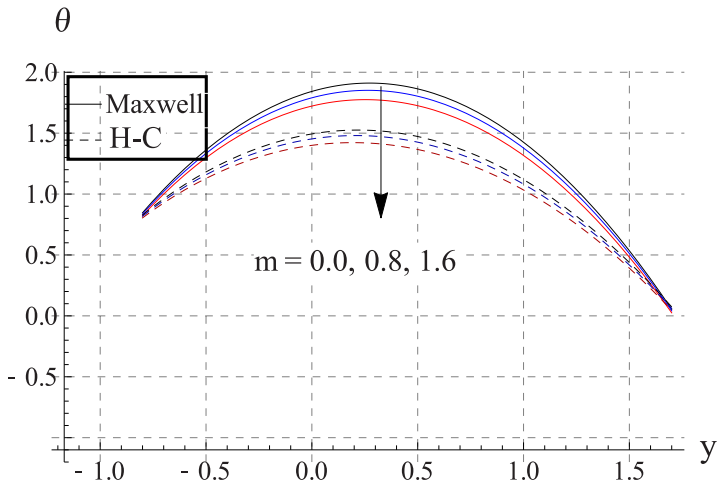

Fig 29. Effect of m on temperature for Al_2O_3 when a = 0.7, b = 0.6, γ = π/2, d = 0.8, x = 0, η = 0.7, Br = 0.3, ϕ = 0.2, M = 2.0, Bi_1 = 8, Bi_2 = 10, Gr = 3.0, ε = 2.5.

doi:10.1371/journal.pone.0153537.g029

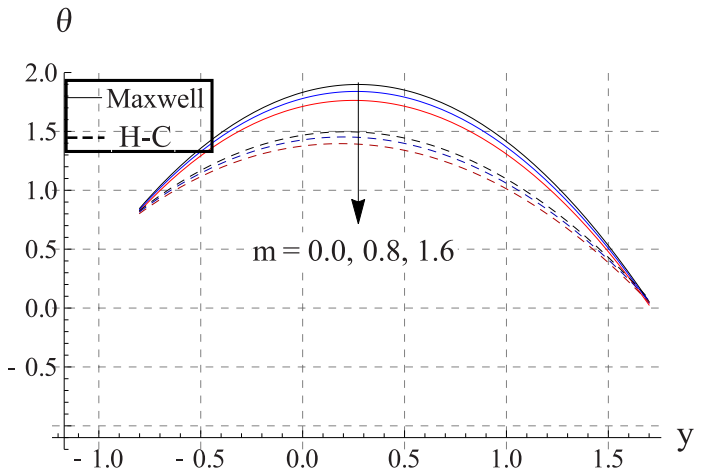

Fig 30. Effect of m on temperature for CuO when a = 0.7, b = 0.6, γ = π/2, d = 0.8, x = 0, η = 0.7, Br = 0.3, ϕ = 0.2, M = 2.0, Bi_1 = 8, Bi_2 = 10, Gr = 3.0, ε = 2.5.

doi:10.1371/journal.pone.0153537.g030

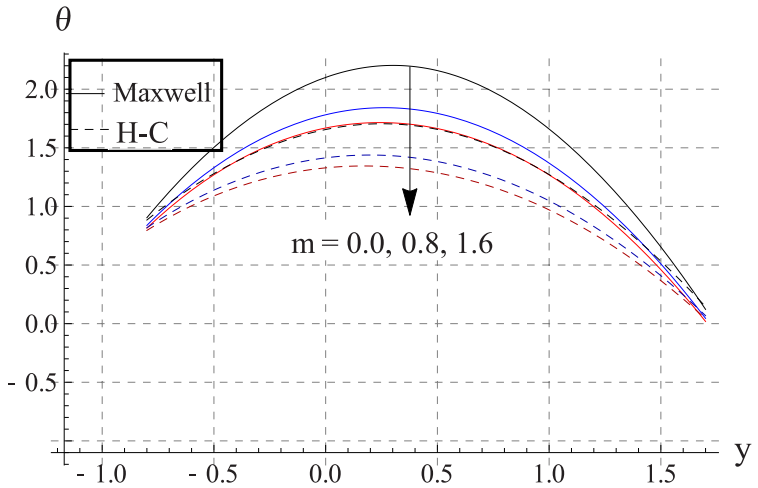

Fig 31. Effect of m on temperature for Cu when a = 0.7, b = 0.6, γ = π/2, d = 0.8, x = 0, η = 0.7, Br = 0.3, ϕ = 0.2, M = 2.0, Bi_1 = 8, Bi_2 = 10, Gr = 3.0, ε = 2.5.

doi:10.1371/journal.pone.0153537.g031

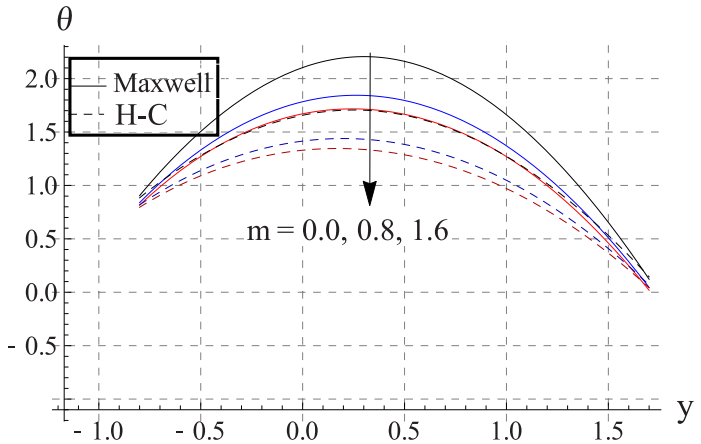

Fig 32. Effect of m on temperature for Ag when a = 0.7, b = 0.6, γ = π/2, d = 0.8, x = 0, η = 0.7, Br = 0.3, ϕ = 0.2, M = 2.0, Bi_1 = 8, Bi_2 = 10, Gr = 3.0, ε = 2.5.

doi:10.1371/journal.pone.0153537.g032

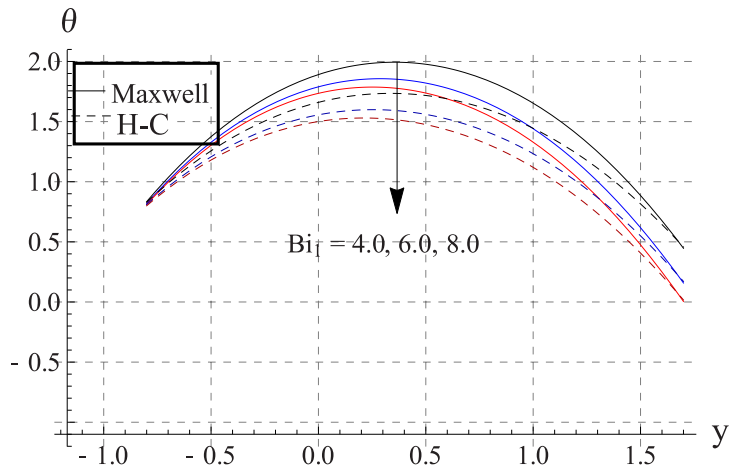

Fig 33. Effect of Bi_1 on temperature for TiO_2 when a = 0.7, b = 0.6, γ = π/2, d = 0.8, x = 0, η = 0.7, Br = 0.3, ϕ = 0.2, m = 2.0, M = 1.0, Bi_2 = 10, Gr = 3.0, ε = 2.5.

doi:10.1371/journal.pone.0153537.g033

Dimensionless form of the walls shape is defined as follows:

$$\begin{aligned} h_1(x) &= 1 + a\cos(2\pi x), \\ h_2(x) &= -d - b\cos(2\pi x + \gamma). \end{aligned} \tag{22}$$

Now the Eqs 14–16 and the boundary conditions Eq (21) are solved by using the NDSolve in MATHEMATICA. The obtained results are analyzed in the next section via graphs and bar charts.

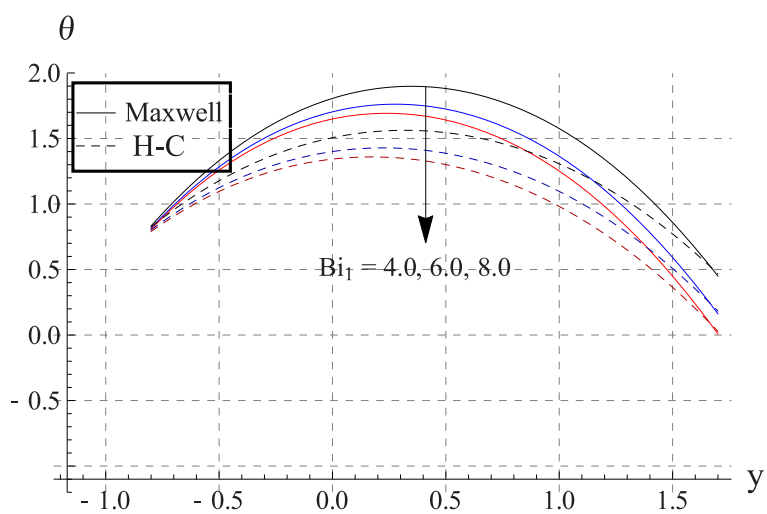

Fig 34. Effect of Bi_1 on temperature for Al_2O_3 when a = 0.7, b = 0.6, γ = π/2, d = 0.8, x = 0, η = 0.7, Br = 0.3, ϕ = 0.2, m = 2.0, M = 1.0, Bi_2 = 10, Gr = 3.0, ε = 2.5.

doi:10.1371/journal.pone.0153537.g034

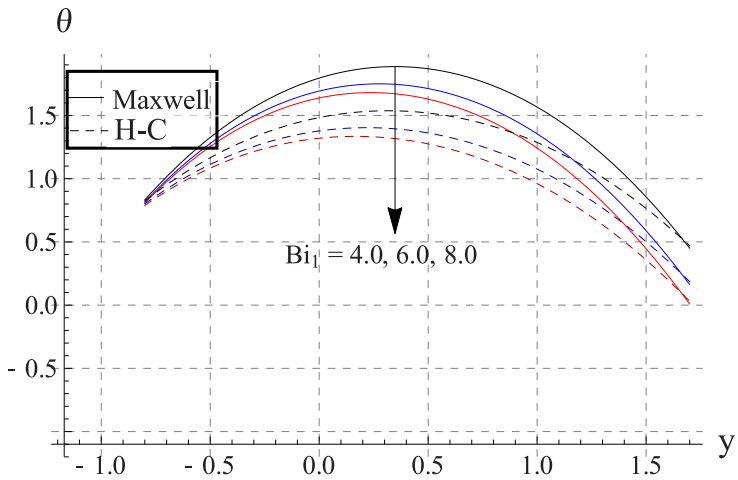

Fig 35. Effect of Bi_1 on temperature for CuO when a = 0.7, b = 0.6, γ = π/2, d = 0.8, x = 0, η = 0.7, Br = 0.3, ϕ = 0.2, m = 2.0, M = 1.0, Bi_2 = 10, Gr = 3.0, ε = 2.5.

doi:10.1371/journal.pone.0153537.g035

Results and Discussion

In this section we investigate the behavior of different water-based nanofluids for different embedded parameters by considering the two thermal conductivity models. Analysis of velocity, temperature and heat transfer rate at the wall is given due attention.

Fig 2 elucidates the effect of volume fraction on the effective thermal conductivity of the various nanofluids consisting of nanoparticles. Higher the effective thermal conductivity is observed for Hamilton-Crosser's model when compared with the Maxwell's model. It is also noticed that the difference between the values get enhanced when we increase the volume fraction ϕ. Moreover for metallic particles such difference is greater than the metallic oxides particles.

Figs 3–7 are prepared to study the impact of volume fraction on velocity for five different nanofluids. We can see that with an increase in volume fraction the velocity of the nanofluid near the center of channel decreases. Maximum velocity is higher for Maxwell's model than H-C's model. Such decrease in maximum value of the velocity is due to an increase in the

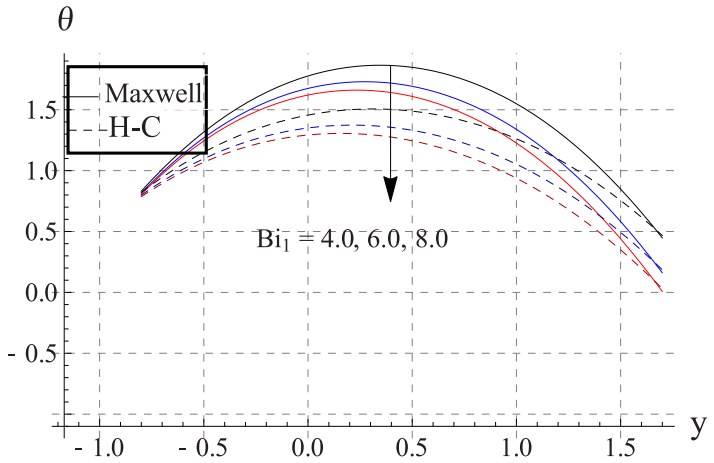

Fig 36. Effect of Bi_1 on temperature for Cu when a = 0.7, b = 0.6, γ = π/2, d = 0.8, x = 0, η = 0.7, Br = 0.3, ϕ = 0.2, m = 2.0, M = 1.0, Bi_2 = 10, Gr = 3.0, ε = 2.5.

doi:10.1371/journal.pone.0153537.g036

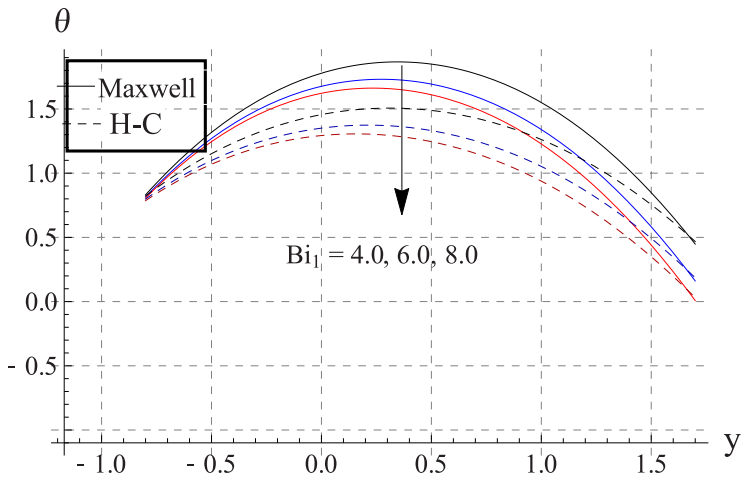

Fig 37. Effect of Bi_1 on temperature for Ag when a = 0.7, b = 0.6, γ = π/2, d = 0.8, x = 0, η = 0.7, Br = 0.3, ϕ = 0.2, m = 2.0, M = 1.0, Bi_2 = 10, Gr = 3.0, ε = 2.5.

doi:10.1371/journal.pone.0153537.g037

resistance produced by increasing the nanoparticle volume fraction ϕ. Infact an increase in nanoparticle volume fraction greatly enhances the viscosity of the nanofluid. This ultimate reduces the maximum velocity. Moreover with an increase in nanoparticle volume fraction the difference between the values of two models increases. Such difference becomes large when thermal conductivity of the nanoparticles is increased.

In order to analyze the impact of volume fraction on temperature, Figs 8–12 are sketched. Increase in volume fraction of nanofluid causes reduction in temperature. The values computed by using the Maxwell's thermal conductivity is greater than the H-C's model. The reason behind such behavior is the fact that an increase in the effective thermal conductivity causes the increase in heat transfer rate across the boundaries. For the cylindrical nanoparticles this heat transfer rate increases more so values of temperature for H-C's model is less than the Maxwell's model. Also the difference between the values of two models is larger when we increase

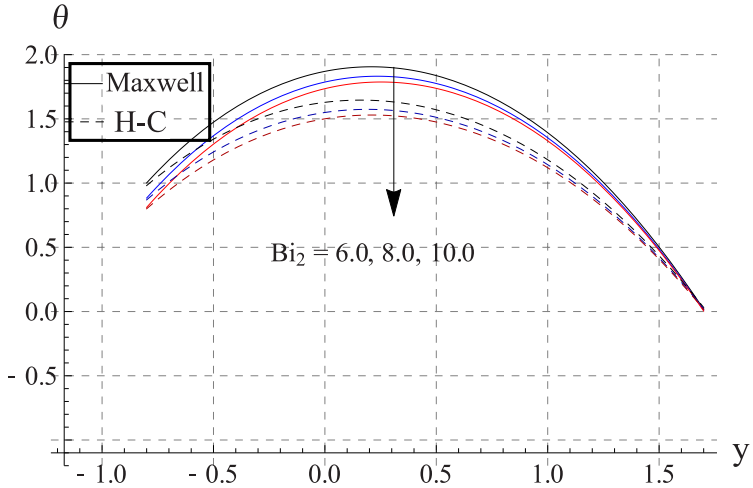

Fig 38. Effect of Bi_2 on temperature for TiO_2 when a = 0.7, b = 0.6, γ = π/2, d = 0.8, x = 0, η = 0.7, Br = 0.3, ϕ = 0.2, m = 2.0, M = 1.0, Bi_1 = 8, Gr = 3.0, ε = 2.5.

doi:10.1371/journal.pone.0153537.g038

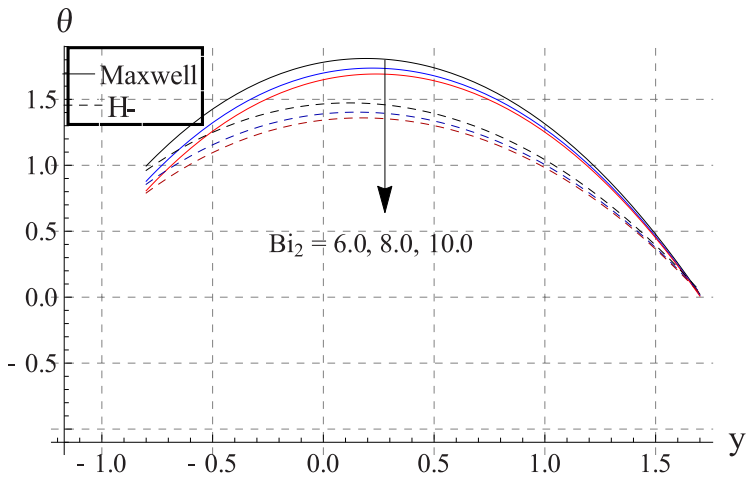

Fig 39. Effect of Bi_2 on temperature for Al_2O_3 when a = 0.7, b = 0.6, γ = π/2, d = 0.8, x = 0, η = 0.7, Br = 0.3, ϕ = 0.2, m = 2.0, M = 1.0, Bi_1 = 8, Gr = 3.0, ε = 2.5.

doi:10.1371/journal.pone.0153537.g039

the nanoparticle volume fraction. Moreover for the particles with high values of thermal conductivities this gap between the values of two models increases.

Figs 13–17 are sketched for the impact of Hartman number on the axial velocity. With increase in Hartman number or increase in the applied magnetic field the maximum velocity of the nanofluid decreases. The resistive nature of magnetic force is responsible for such behavior. The difference between the values of the two models is enhanced when the values of magnetic field strength and thermal conductivity are increased.

Figs 18–22 study the impact of Hartman number on the temperature. We observed that with an increase in the magnetic field strength the temperature of the nanofluid increases. Such increase in the temperature results from Ohmic heating (Joule heating). Also difference between two models increases with an increase in applied magnetic field. Such difference is greater for the metallic nanoparticles than the metallic oxides ones.

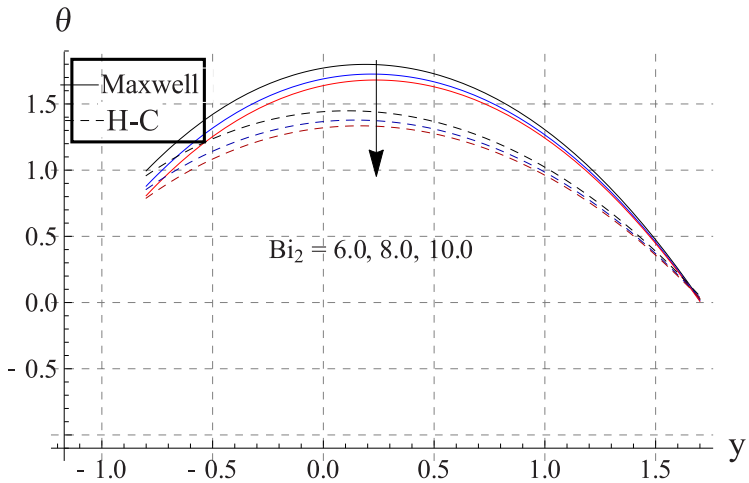

Fig 40. Effect of Bi_2 on temperature for CuO when a = 0.7, b = 0.6, γ = π/2, d = 0.8, x = 0, η = 0.7, Br = 0.3, ϕ = 0.2, m = 2.0, M = 1.0, Bi_1 = 8, Gr = 3.0, ε = 2.5.

doi:10.1371/journal.pone.0153537.g040

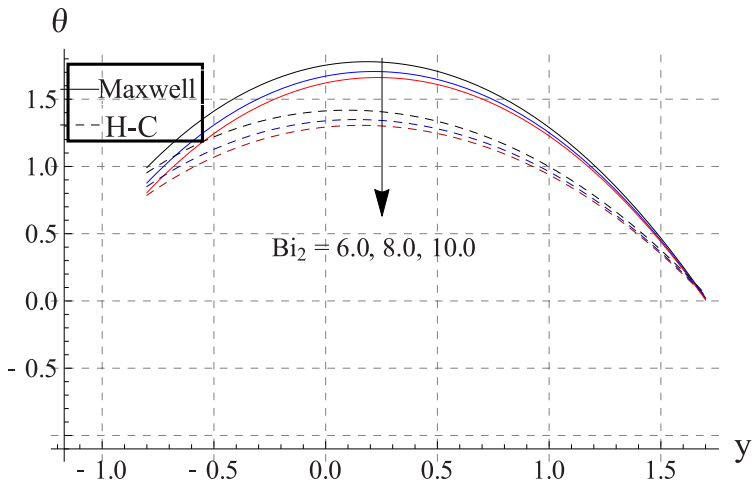

Fig 41. Effect of Bi_2 on temperature for Cu when a = 0.7, b = 0.6, γ = π/2, d = 0.8, x = 0, η = 0.7, Br = 0.3, ϕ = 0.2, m = 2.0, M = 1.0, Bi_1 = 8, Gr = 3.0, ε = 2.5.

doi:10.1371/journal.pone.0153537.g041

Figs 23–27 show the behavior of Hall parameter on velocity. We noticed that maximum velocity of nanofluid increases for larger Hall parameter. This indicates that the Hall parameter resists the change in the fluid caused by an increase in the strength of applied magnetic field. In all of the above mentioned quantities the value of Maxwell's model is greater than the H-C's model. Furthermore the difference between the two models is larger when we increase the thermal conductivity of the nanoparticles.

Hall parameter describes opposite behavior on temperature than Hartman number (see Figs 28–32. Decrease in temperature is observed for an increase in the Hall parameter. It depicts that the Hall parameter resists the enhancement in the nanofluid temperature brought by an increase in the strength of applied magnetic field. Note that in all cases the value of Maxwell's

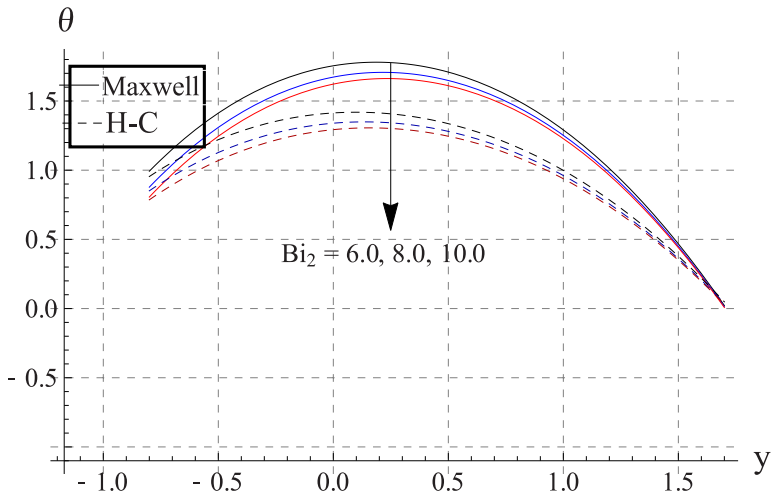

Fig 42. Effect of Bi_2 on temperature for Ag when a = 0.7, b = 0.6, γ = π/2, d = 0.8, x = 0, η = 0.7, Br = 0.3, ϕ = 0.2, m = 2.0, M = 1.0, Bi_1 = 8, Gr = 3.0, ε = 2.5.

doi:10.1371/journal.pone.0153537.g042

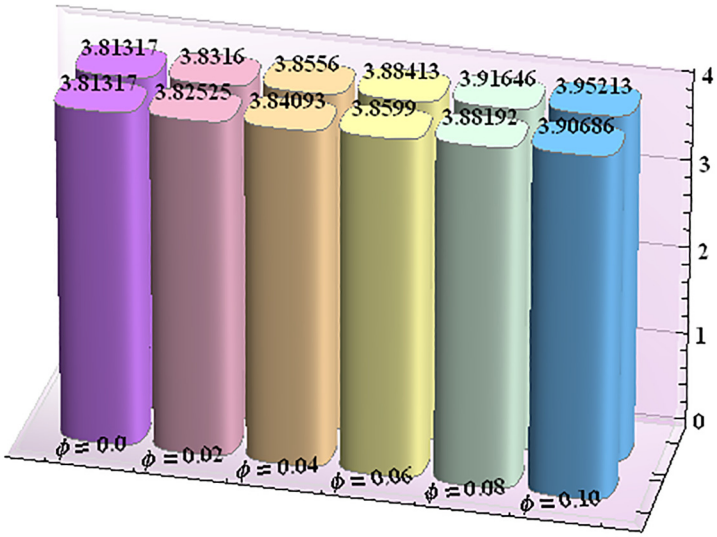

Fig 43. Effect of ϕ on the heat transfer rate at the wall $\left(-\frac{K_{eff}}{K_f}\theta'(h_1)\right)$ for TiO_2-water nanofluid when a = 0.7, b = 0.6, γ = π/2, d = 0.8, x = 0, η = 0.7, Br = 0.3, m = 0.8, M = 1.0, Bi_1 = 8, Bi_2 = 10, Gr = 3.0, ε = 2.5.

doi:10.1371/journal.pone.0153537.g043

model is greater than the Hamilton-Crosser's model. Moreover the difference between the two models is larger when we increase the thermal conductivity of the nanoparticles.

Figs 33–42 describe the impact of Biot numbers on the temperature. Increasing the values of Biot numbers reduces the temperature of the nanofluid. The values for Maxwell's model are greater in comparison to H-C's model. Furthermore the difference between the two models is larger when we increase the thermal conductivity of the nanoparticles.

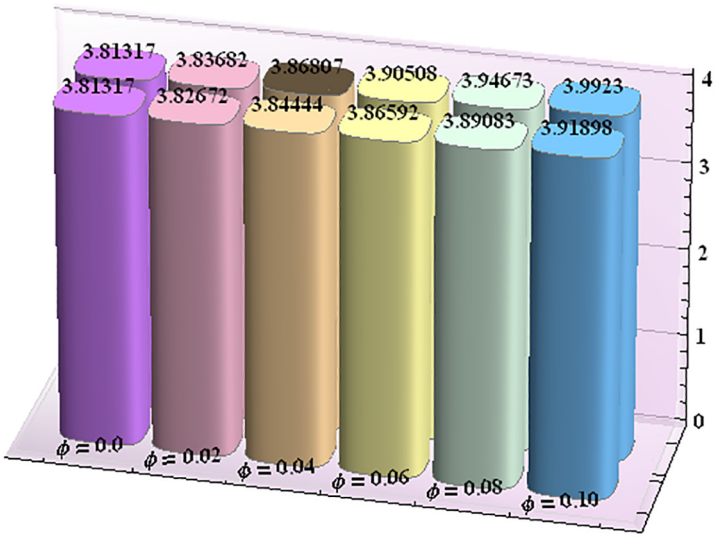

Fig 44. Effect of ϕ on the heat transfer rate at the wall $\left(-\frac{K_{eff}}{K_f}\theta'(h_1)\right)$ for Al_2O_3-water nanofluid when a = 0.7, b = 0.6, γ = π/2, d = 0.8, x = 0, η = 0.7, Br = 0.3, m = 0.8, M = 1.0, Bi_1 = 8, Bi_2 = 10, Gr = 3.0, ε = 2.5.

doi:10.1371/journal.pone.0153537.g044

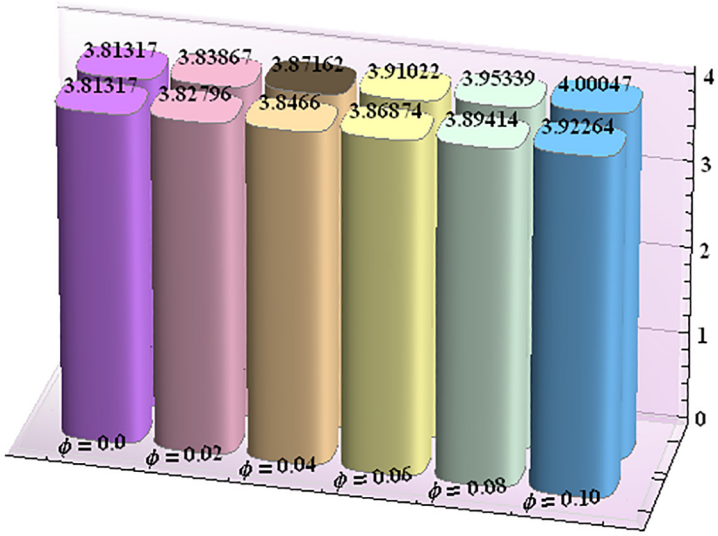

Fig 45. Effect of ϕ on the heat transfer rate at the wall $\left(-\frac{K_{eff}}{K_f}\theta'(h_1)\right)$ for CuO-water nanofluid when a = 0.7, b = 0.6, γ = π/2, d = 0.8, x = 0, η = 0.7, Br = 0.3, m = 0.8, M = 1.0, Bi_1 = 8, Bi_2 = 10, Gr = 3.0, ε = 2.5.

doi:10.1371/journal.pone.0153537.g045

Figs 43–47 portray the impact of nanoparticle volume fraction on the rate of heat transfer at the wall. Study discloses the fact that the heat transfer rate at the wall is increasing function of nanoparticle volume fraction ϕ. For H-C's model the heat transfer rate is higher than the Maxwell's model. Moreover rate of heat transfer is increased by enhancing the thermal conductivity of nanoparticles. Also by an increase in volume fraction the gap between the values of two models widens.

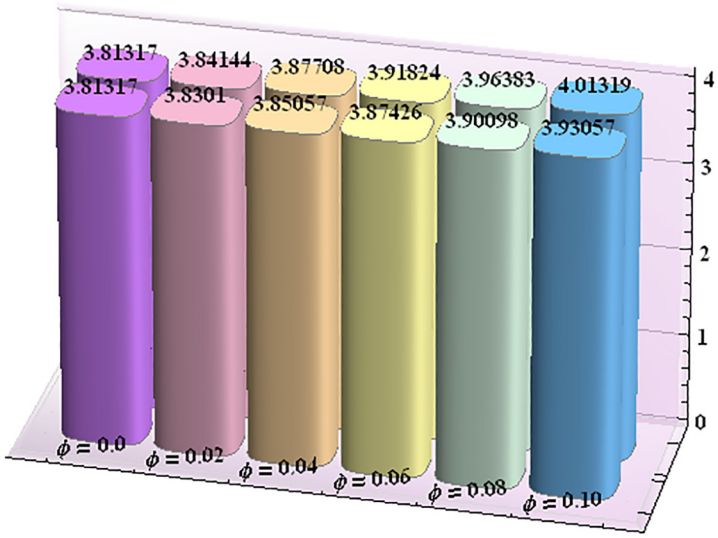

Fig 46. Effect of ϕ on the heat transfer rate at the wall $\left(-\frac{K_{eff}}{K_f}\theta'(h_1)\right)$ for Cu-water nanofluid when a = 0.7, b = 0.6, γ = π/2, d = 0.8, x = 0, η = 0.7, Br = 0.3, m = 0.8, M = 1.0, Bi_1 = 8, Bi_2 = 10, Gr = 3.0, ε = 2.5.

doi:10.1371/journal.pone.0153537.g046

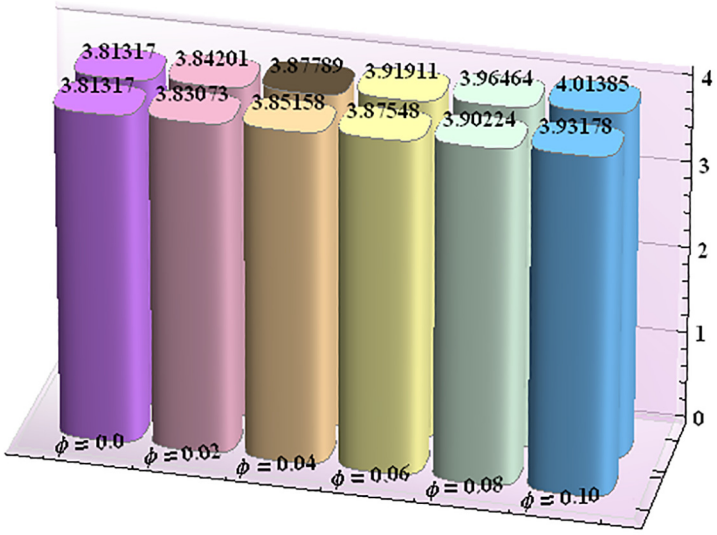

Fig 47. Effect of ϕ on the heat transfer rate at the wall $\left(-\frac{K_{eff}}{K_f}\theta'(h_1)\right)$ for Ag-water nanofluid when a = 0.7, b = 0.6, γ = π/2, d = 0.8, x = 0, η = 0.7, Br = 0.3, m = 0.8, M = 1.0, Bi_1 = 8, Bi_2 = 10, Gr = 3.0, ε = 2.5.

doi:10.1371/journal.pone.0153537.g047

Conclusions

Here we analyzed the MHD mixed convection peristaltic transport of water-based nanofluids by employing convective conditions on the channel boundaries. The following observations are worth mentioning.

- By nanoparticle volume fraction, both the axial velocity and temperature are decreased. Increasing the nanoparticles the difference between the values of two models increases. Such increase is larger for metallic particles.
- By increasing the strength of magnetic field the velocity of nanofluid decreases. Larger strength of magnetic field increased the difference between the two models. For metallic particles this gap widens than metallic oxides.
- By increasing the strength of magnetic field the temperature of nanofluid increases in view of Joule heating. Increasing strength of magnetic field enhanced the difference between the two models. For metallic particles this gap is more than metallic oxides.
- Hartman number and Hall parameter shows opposite behavior on the velocity and temperature.
- With an increase in the Biot number the temperature of the nanofluid decreases. For the nanoparticles with high thermal conductivity the difference between the values of two models is large.
- Heat transfer rate at the wall enhances with increasing nanoparticle volume fraction. Moreover such increase is larger for cylindrical nanoparticles than the spherical ones.

Acknowledgments

The contributing members of NAAM group:

1. Prof Dr Tasawar Hayat
2. Prof Dr Ahmad Alsaedi

Author Contributions

Conceived and designed the experiments: TH SN AA MR. Performed the experiments: TH SN AA MR. Analyzed the data: TH SN AA MR. Contributed reagents/materials/analysis tools: TH SN AA MR. Wrote the paper: TH SN AA MR.

References

1. Choi SUS, Enhancing thermal conductivity of the fluids with nanoparticles. ASME Fluids Eng Div. 1995; 231: 99–105.
2. Lin Y, Zheng L, Zhang X, Ma L, Chen G, MHD pseudoplastic nanofluid unsteady flow and heat transfer in a finite thin film over stretching surface with internal heat generation. Int J Heat Mass Transfer. 2015; 84: 903–911.
3. Buongiorno J, Convective transport in nanofluids. ASME J Heat Transfer. 2006; 128: 240–250.
4. Turkyilmazoglu M, Nanofluid flow and heat transfer due to a rotating disk. Comput Fluids. 2014; 94: 139–146.
5. Abbasi FM, Hayat T, Ahmad B, Chen GQ, Peristaltic motion of non-Newtonian nanofluid in an asymmetric channel. Z Naturforsch. 2014; 69a: 451–461.
6. Turkyilmazoglu M, The analytical solution of mixed convection heat transfer and fluid flow of a MHD viscoelastic fluid over a permeable stretching surface. Int J Mechanical Science. 2013; 77: 263–268.
7. Sheikholeslami M, Ganji DD, Javed MY, Ellahi R, Effect of thermal radiation on magnetohydrodynamics nanofluid flow and heat transfer by means of two phase model. J Magn Magn Mater. 2015; 374: 36–43.
8. Khan JA, Mustafa M, Hayat T, Alsaedi A, Three-dimensional flow of nanofluid over a nonlinearly stretching sheet: An application to solar energy. Int J Heat Mass Transfer. 2015; 8: 158–164.
9. Akram S, Nadeem S, Consequence of nanofluid on peristaltic transport of a hyperbolic tangent fluid model in the occurence of apt (tending) magnetic field. J Magn Magn Mater. 2014; 358: 183–191.
10. Ebdid A, Remarks on the homotopy perturbation method for the peristaltic flow of Jeffrey fluid with nanoparticles in an asymmetric channel. Comp Math Appl. 2014; 68 (3): 77–85.
11. Maxwell JC, A Treatise on Electricity and Magnetism. 2nd Edition Oxford University Press, Cambridge. 1904; 435–441.
12. Hamilton RL, Crosser OK, Thermal conductivity of heterogeneous two component systems. EC Fundam. 1962; 1 (3): 187–191.
13. Shapiro AH, Pumping and retrograde diffusion in peristaltic waves, In Proc Workshop Ureteral Reftm Children. Nat Acad Sci, Washington, DC. 1967; 1: 109–126.
14. Weinberg SL, Theoretical and experimental treatment of peristaltic pumping and its relation to ureteral function. PhD Thesis, MIT, Cambridge, MA. 1970.
15. Asghar S, Hussain Q, Hayat T, Peristaltic motion of reactive viscous fluid with temperature dependent viscosity. Math Comp App. 2013; 18 (3): 198–220.
16. Mekheimer KHS, Elmaboud YABD, Abdellateef AI, Particulate suspension flow induced by sinusoidal peristaltic waves through eccentric cylinders: thread annular. Int J Biomath. 2013; 6 (4): 1350026.
17. Hayat T, Rafiq M, Ahmad B, Combined effects of rotation and thermal radiation on peristaltic transport of Jeffrey fluid. Int J Biomath. 2015; 8 (5): 21 pages.
18. Hayat T, Rafiq M, Ahmad B, Radiative and Joule heating effects on peristaltic transport of dusty fluid in a channel with wall properties. Eur Phys J Plus. 2015; 129: 225.
19. Abbasi FM, Hayat T, Alsaedi A, Numerical analysis for MHD peristaltic transport of Carreau-Yasuda fluid in a curved channel with Hall effects. J Magn Magn Mater. 2015; 382: 104–110.
20. Srinivas S, Kothandapani M, Peristaltic transport in an asymmetric channel with heat transfer—A note. Int Commun Heat Mass Transfer. 2008; 35 (4): 514–522.
21. Hina S, Mustafa M, Hayat T, Alsaadi FE, Peristaltic motion of third grade fluid in curved channel. App Math Mech Engl Ed. 2014; 35 (1): 73–84.

22. Hayat T, Abbasi FM, Ahmad B, Alsaedi A, Peristaltic transport of Carreau-Yasuda fluid in a curved channel with slip effects. Plos One. 2014; 9 (4): e95070. doi: 10.1371/journal.pone.0095070 PMID: 24736320
23. Hayat T, Abbasi FM, Ahmad B, Alsaedi A, MHD mixed convection peristaltic flow with variable viscosity and thermal conductivity. Sains Malays. 2014; 43 (10): 1583–1590.
24. Ali N, Javed T, Flow of a Giesekus fluid in a planar channel due to peristalsis. Z Naturforsch. 2013; 68a: 515–523.
25. Ellahi R, Hussain F, Simultaneous effects of MHD and partial slip on peristaltic flow of Jeffrey fluid in a rectangular duct. J Magn Magn Mater. 2015; 393: 284–292.
26. Hayat T, Tanveer A, Alsaadi F, Alotaibi ND, Homogeneous-hetrogeneous reaction effects in peristalsis through curved channel geometry. AIP Advances. 2015; 5: 067172.
27. Shehzad SA, Abbasi FM, Hayat T, Alsaadi F, MHD mixed convective peristaltic motion of nanofluid with Joule heating and thermophoresis effects. Plos One. 2014; 9 (11): e111417. doi: 10.1371/journal.pone.0111417 PMID: 25391147
28. Hayat T, Abbasi FM, Al-Yami M, Monaquel S, Slip and Joule heating effects in mixed convection peristaltic transport of nanofluid with Soret and Dufour effects. J Mol Liq. 2014; 194: 93–99.
29. Abbasi FM, Hayat T, Ahmad B, Chen GQ, Slip effects on mixed convective peristaltic transport of copper-water nanofluid in an inclined channel. Plos One. 2014; 9 (8): e105440. doi: 10.1371/journal.pone.0105440 PMID: 25170908
30. Abbasi FM, Hayat T, Alsaedi A, Peristaltic transport of magneto-nanoparticles submerged in water: Model for drug delivery system. Physica E: Low-dimensional Systems and Nanostructures. 2015; 68: 123–132.
31. Abbasi FM, Hayat T, Ahmad B, Impact of magnetic field on mixed convective peristaltic flow of water based nanofluids with Joule heating. Z Naturforsch. 2015; 70 (2): 125–132.
32. Abbasi FM, Hayat T, Ahmad B, Peristalsis of silver-water nanofluid in the presence of Hall and Ohmic heating effects: Applications in drug delivery. J Mol Liq. 2015; 207: 248–255.
33. Abbasi FM, Hayat T, Ahmad B, Peristaltic transport of copper-water nanofluid saturating porous medium. Physica E: Low-dimensional Systems and Nanostructures. 2015; 67: 47–53.
34. Shehzad SA, Abbasi FM, Hayat T, Alsaadi F, Model and comparative study for the peristaltic transport of water based nanofluids. J Mol Liq. 2015; 209: 723–728.
35. Abbasi FM, Hayat T, Ahmad B, Peristaltic flow in an asymmetric channel with convective boundary conditions and Joule heating. J Cent South Univ. 2014; 21 (4): 1411–1416.